

High ice-nucleating particle concentrations associated with Arctic haze in springtime cold-air outbreaks

Erin N. Raif¹, Sarah L. Barr^{1,2}, Mark D. Tarn¹, James B. McQuaid¹, Martin I. Daily¹, Steven J. Abel⁴, Paul A. Barrett⁴, Keith N. Bower³, Paul R. Field^{1,4}, Kenneth S. Carslaw¹, and Benjamin J. Murray¹

¹University of Leeds, Woodhouse Road, Leeds, LS2 9JT, UK

²National Centre for Atmospheric Science, Clarendon Road, Leeds, LS2 9PH, UK

³University of Manchester, Oxford Road, Manchester, M13 9PL, UK

⁴Met Office, FitzRoy Road, Exeter, EX1 3PB, UK

Correspondence: Erin N. Raif (eenr@leeds.ac.uk)

Abstract. The global variation of ice-nucleating particle (INP) concentrations is an important modulator of the cloud-phase feedback, where the albedo of mixed-phase clouds increases in a warming climate. Shallow clouds such as those observed in cold-air outbreaks (CAOs) are particularly important for cloud-phase feedbacks and highly sensitive to INPs. To investigate the sources and concentrations of INPs in CAOs, we made airborne measurements over the Norwegian and Barents seas as part of the March 2022 Arctic Cold-Air Outbreak (ACAO) field campaign. Aerosol samples were collected on filters at locations above, below and [upwind-upstream](#) of CAO cloud decks. Throughout the campaign, INP concentrations were comparable to the highest previously observed in the Arctic. Scanning electron microscopy analysis of samples taken [upwind-upstream](#) of cloud decks showed that super-micron aerosol was dominated by mineral dusts. Analysis of aerosol particle size measurements to obtain an INP active site density suggested sea spray was unlikely to be the dominant INP type. These site densities were also too great for mineral components alone to be the dominant INP type above -20 °C. Accordingly, it is likely that the dominant INP type was mineral dust mixed with other ice nucleating materials, possibly of biogenic origin. Back-trajectory analysis and meteorological conditions suggested a lack of local INP sources. We therefore hypothesise that the high INP concentration is most likely to be associated with aged aerosol in Arctic haze that has undergone long-range transport from lower latitude regions.

1 Introduction

Marine cold-air outbreaks (CAOs) are frequent high-intensity weather events in the mid- to high-latitudes where cold polar air is drawn equatorwards over an increasingly warmer ocean (Fletcher et al., 2016b). The relative warmth of the ocean compared to the airmass causes the polar [airmass-air](#) to become warmer and more moist, resulting in extensive mixed-phase cloud systems (Brümmer, 1996; Fletcher et al., 2016a; Abel et al., 2017). In these cloud systems, stratiform clouds form at the sea-ice edge, which transition into open cumulus cells as the airmass moves equatorward. These often take the form of “cloud streets”, streaks of stratocumulus cloud in the direction of the prevailing wind (Pithan et al., 2018; Murray-Watson et al., 2023).

The presence of supercooled liquid water in these mixed-phase CAO clouds makes them sensitive to the presence of ice-nucleating particles (INPs). INPs are a subset of aerosol that allow droplets of supercooled liquid water in clouds to freeze at temperatures above $-35\text{ }^{\circ}\text{C}$ (Murray et al., 2012b; Kanji et al., 2017), where homogeneous freezing does not occur at appreciable rates (Ickes et al., 2015; Herbert et al., 2015). Globally significant INP species include mineral dust, sea-spray aerosol and biological material such as bacteria and fungal spores (Kanji et al., 2017). Where ice and liquid coexist in mixed-phase clouds, ice particles are able to grow by vapour deposition at the expense of liquid droplets since the saturation vapour pressure over liquid is greater than the saturation vapour pressure over ice (Wegener, 1911). ~~Since ice crystal concentrations are typically lower than liquid droplet concentrations in mixed-phase clouds~~ Through this process, ice crystals are able to grow ~~through this process~~ to sizes at which they can precipitate, enhancing precipitation (Bergeron, 1935; Findeisen, 1938). Since ice crystal concentrations are typically lower than liquid droplet concentrations in mixed-phase clouds, this process can be highly efficient. Ice crystals that have formed through ice nucleation may also grow by subsequent microphysical processes such as riming, where supercooled droplets are collected by ice crystals. Additionally the ice crystal concentration may increase by secondary ice processes such as rime splintering (Field et al., 2017; Hallett and Mossop, 1974; Korolev and Leisner, 2020). Consequently, the concentration of INPs can act as a strong control on the ratio of liquid and ice in a mixed-phase cloud.

Since increased proportions of ice are associated with reduced albedo, the concentration of INPs can influence the albedo of the cloud (Garrett et al., 2001; Korolev et al., 2017). In simulations of a Southern Hemisphere CAO, Vergara-Temprado et al. (2018) showed that the reflectivity of clouds in CAO systems decreases with increasing INP concentration since low INP concentrations suppressed droplet freezing and precipitation and increased cloud lifetime. Additionally, simulations of a Northern Hemisphere CAO by Abel et al. (2017) showed that precipitation can influence the rate of cloud transition between the more reflective stratiform state and the less reflective cumuliform state, while simulations of CAOs by Tornow et al. (2021) have shown that INPs can influence the onset of precipitation and thus the initiation of the reduction in cloud cover due to the cloud transition. In a warming climate, ice crystals in mixed-phase clouds will be susceptible to replacement by liquid water, increasing cloud albedo resulting in a cooling feedback (Storelvmo et al., 2015). Since INP concentration can modulate the concentration of ice, the availability of INPs in CAO clouds could influence the magnitude of this cloud-phase feedback (Murray et al., 2021). The cloud-phase feedback is likely to be particularly sensitive to CAO clouds since they form over the relatively dark ocean, so microphysical adjustments to cloud albedo have the potential to be more impactful than for clouds over higher-albedo surfaces such as sea ice.

INP concentrations vary substantially both spatially and temporally, but some of the greatest variability observed anywhere on Earth occurs in the Arctic. Measurements of INPs in the Arctic reveal some of the lowest INP concentrations on Earth, comparable with the Southern Ocean, to some of the greatest, comparable with mid-latitude locations where terrestrial biological INP types dominate (Murray et al., 2021). Variability occurs ~~on both~~ both on seasonal scales (Wex et al., 2019; Sze et al., 2023) and strongly on timescales of hours to days (Porter et al., 2022). This indicates that the sources of INPs within and transported to the Arctic are variable, but also that removal processes are important, since periods of high INP concentration can be followed by periods of low INP concentration.

Figure 1a shows the potential sources of INPs for CAO clouds in the Northern Hemisphere. Potential Arctic sources of INPs are biogenic material from sea-spray (Wilson et al., 2015; DeMott et al., 2016; McCluskey et al., 2018b) and terrestrial INPs from high-latitude sources (Kawai et al., 2023). Potential terrestrial sources of INP include glacial outwash sediments (Tobo et al., 2019; Xi et al., 2022; Barr et al., 2023), sandy deserts in Iceland (Sanchez-Marroquin et al., 2020), boreal forests (Brasseur et al., 2022), [Arctic surface vegetation \(Pereira Freitas et al., 2023\)](#) and thawing permafrost (Creamean et al., 2020). In addition, Arctic aerosol can have lifetimes of many weeks, which results in ~~th~~the build-up of Arctic Haze in winter and spring (Stohl, 2006). Accordingly, it is also possible that INPs entering CAOs may have been transported into the Arctic from lower-latitudes where they reside in the stable Arctic atmosphere before being transported out again in CAOs (Carslaw, 2022). ~~Since different~~ Different types of INPs have different characteristic ranges of freezing temperatures (Kanji et al., 2017). ~~This~~ This means understanding the aerosol sources that contribute to the INP population in CAO clouds can reduce the uncertainty in the cloud-phase feedback.

To understand the sources of INPs into CAO clouds, there is a need for localised airborne aerosol measurements to capture INP concentrations throughout a cold-air outbreak, especially in the Northern Hemisphere. Previously, Northern Hemisphere aircraft campaigns have characterised the dynamics of cold-air outbreaks (Brümmer, 1996) over the Norwegian Sea and made airborne measurements of aerosol and cloud without INP measurements in mid-latitude cold-air outbreak conditions (Young et al., 2016; Sorooshian et al., 2019). INP measurements have been made in CAOs from the ground in the northern hemisphere (~~Geerts et al., 2022~~) ([Geerts et al., 2022](#); [Gjelsvik et al., 2024](#)) and from aircraft in the the Southern Hemisphere (McFarquhar et al., 2021; McCluskey et al., 2018a). In this study, we focus on cold-air outbreaks over the Norwegian and Barents seas to report the first airborne measurements of INPs in Northern Hemisphere cold-air outbreaks. Having reported these measurements, we characterise the INP concentrations observed and try to identify the primary INP source(s) through a process of elimination of potential sources.

2 Methodology

2.1 The Arctic Cold-Air Outbreak campaign

The Arctic Cold-Air Outbreak flight campaign (ACAO) took place over the Norwegian and Barents seas in March 2022. The campaign used the BAe-146 aircraft of the Facility for Airborne and Atmospheric Measurement (FAAM) to make measurements in cold-air outbreaks. A key aim was to investigate the development and evolution of the cloud systems and the associated aerosol and cloud microphysical properties. Twelve flights were performed over nine days between 11 March 2022 and 30 March 2022. The tracks of these flights are depicted in Figure 1c. Where possible, flight days and locations were chosen to capture cold-air outbreaks with characteristics such as cloud streets that were clearly positioned away from fronts to ensure well-defined air flows and airmasses. ~~Cold-air outbreak~~ CAO conditions, of varying strength, occurred on eight of the nine flying days. On the other day (flight ~~e272~~c272), a warm-air intrusion (an injection of mid-latitude air into the Arctic (Pithan et al., 2018)) occurred and was measured as a contrasting case. Flights ~~e271 and e273~~ c271 and c273 probed CAOs with westerly flows with air flowing off Greenland, while the flow during ~~e274~~ c274 was northwesterly. Flights ~~e275–e282~~ c275–c282

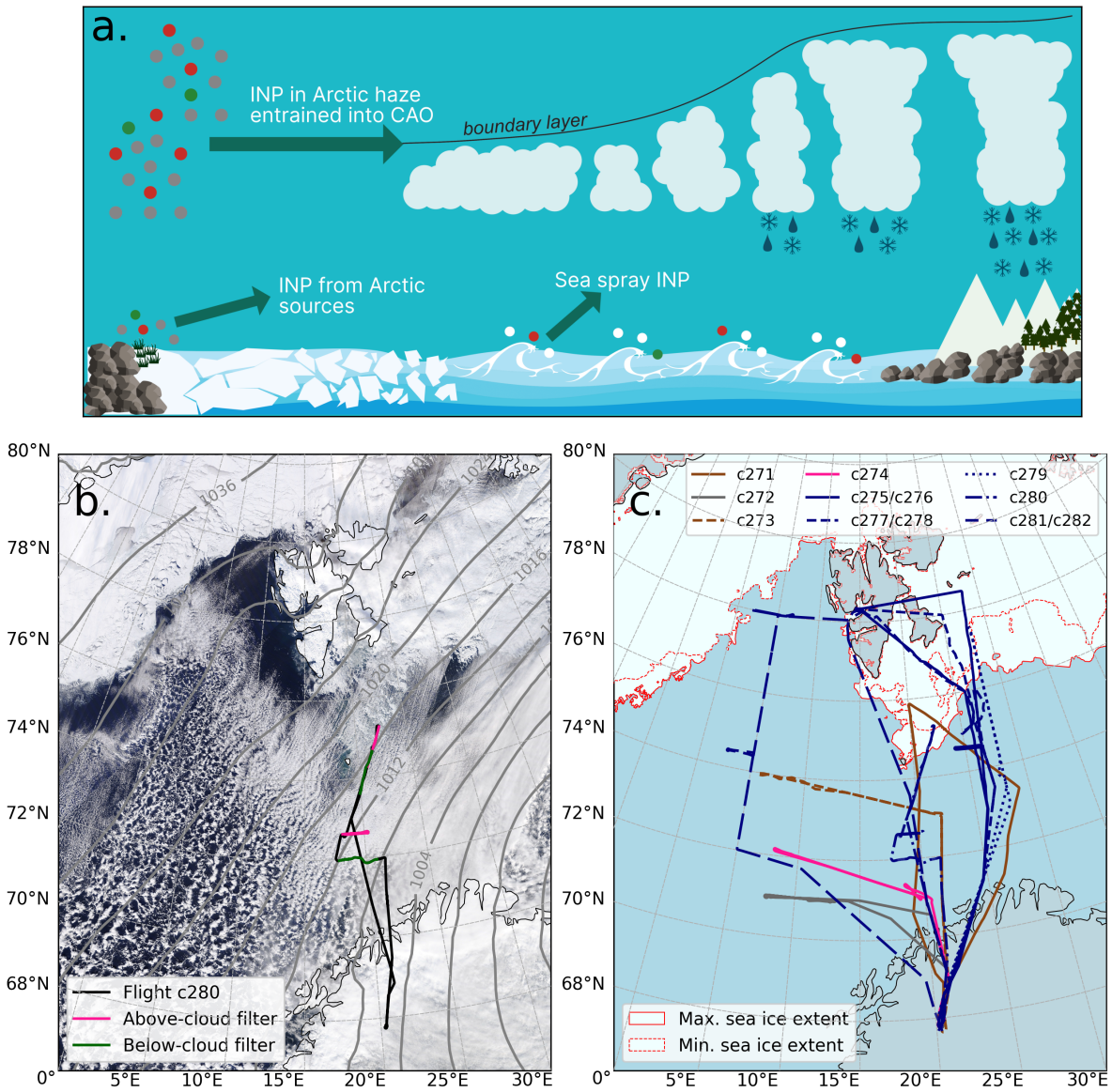


Figure 1. Panel a shows a schematic representation of an Arctic cold-air outbreak and the potential sources of aerosol to the cloud system. Stratiform cloud forms off the sea-ice edge Green and develops into cumulus cloud as the CAO airmass moves south. Biological and abiological INP are represented by green and red circles depict biological and abiological INPs respectively, while grey and white circles depict aerosols that do not actively nucleate ice in CAOs are represented by grey and white circles. Panel b shows a satellite image imagery taken on 30-29 March 2022 by the Moderate Resolution Resolution Imaging Spectroradiometer (MODIS) of a typical CAO measured during the ACAO campaign (MODIS Land Science Team, 2020). The path of flight c280, which probed this CAO, is overlaid along with the locations of INP filter samples, which were taken between 30 min and 2 h before the image time. Sea-level pressure isobars from ERA5 reanalysis are also overlaid (C3S, 2018). Panel c shows flight tracks paths from the all nine flying days during the campaign. Blue, pink and brown flight paths represent CAOs with predominantly N, NW and W flows respectively. Flight c272 probed a warm-air intrusion and is coloured grey. Sea-ice extent in this and other maps was obtained from the Multisensor Analyzed Sea Ice Extent dataset (U.S. National Ice Center et al., 2010). The flight track for flight e278 c278 is incomplete due to equipment failure.

probed CAOs with northerly or north by northeasterly flows. Aerosol measurements were made online (i.e. continuously) using
90 under-wing optical probes and filter samples were collected for specific periods for ~~later~~ subsequent offline analysis.

2.2 Filter samples for INP analysis

~~Filter-~~ In this system, filter samples were collected using the aircraft inlet system characterised by Sanchez-Marroquin et al. (2019). Two parallel inlets are aligned with the heading of the aircraft and the airflow through each inlet is assisted by a vacuum pump. The inlet system is designed to minimise turbulence and flow separation when flying at low Mach number (Andreae
95 et al., 1988, 2000) and has a bypass to remove droplets and ice crystals (Talbot et al., 1990). The bypass also increases the flow rate, reducing the sub-isokinetic enhancement of larger particles (Sanchez-Marroquin et al., 2019). A different type of filter was used in each inlet ~~in order so~~ that different types of analysis could be performed on aerosol samples from the same location and time. Polytetrafluoroethylene (PTFE) membrane filters were used for INP concentration measurements via droplet freezing assays, while polycarbonate track-etched membrane filters were used for scanning electron microscopy with energy
100 dispersive X-ray spectroscopy (SEM-EDS) aerosol composition analysis.

Air entering each inlet passes through a sampling line into a filter holder previously described by Price et al. (2018) and Sanchez-Marroquin et al. (2019). Air that passes through the filter holder is measured by a mass flow meter, which reports the flow in standard litres (273.15 K, 101.325 kPa). Inside the filter holder, the filter sits on a stainless steel support mesh. The PTFE filter (*Sartorius*, product number 11803-47-N) had pore size 1.2 μm , while the polycarbonate filter (*Whatman*, product
105 number 111107) had pore size 0.4 μm . The PTFE filter allowed more throughput for INP analysis while the polycarbonate filter had less throughput. Two types of steel mesh were used during the campaign - one manufactured by *Millipore* (product number XX4304707) and one manufactured by *MesaLabs* (product number 1584). Using the *MesaLabs* meshes enhanced the flow through the filter, though flow rates were consistently greater through PTFE filters than polycarbonate filters. Flow through the filter was also dependent on altitude, with higher flow rates at lower altitudes. The largest volume of air sampled
110 by a PTFE filter was (1730 ± 30) L, while the smallest volume of air sampled was (473 ± 9) L. For polycarbonate filters, the largest volume sampled was (990 ± 20) L, while the smallest was (276 ± 6) L. There was no correlation between the INP concentrations measured and the volume of air sampled by each filter. Handling blanks were collected to determine the baseline ice-nucleating activity of the procedure and equipment used. ~~This was achieved~~ These handling blanks were collected during the flight by loading filters as normal into the aircraft filter holder system, opening the filter system up to air flow for 1–2 s,
115 then closing the filter system and removing the filters as normal. Handling blank filters were processed for INP analysis in the same manner as the aerosol sample filters.

Figure 2a shows the location of the filter sample measurements over the Norwegian and Barents seas between 71–79°N. The altitude of filter measurements was between ~~10–4000~~ 40–3400 m and all samples were taken in air with no cloud or precipitation. The majority of samples were taken above or below the CAO clouds, although two samples (~~c276r2 and c278r2~~ c276r2 and c278r2) were taken upstream of the cloud onset. Sampling periods were ~~approximately 20~~ typically between 18–28 min excluding pauses in sampling where the inlets were temporarily closed when the aircraft turned or flew through precipitation. Only one of the samples (c273r2) had a shorter sampling time of 14 min, while one of the samples (c273r1) had a longer

sampling time of 37 min. However, both of these filters sampled volumes of air that were not at the extremities of the volume range sampled.

125 To derive INP concentrations from the samples, droplet freezing assays were performed according to a drop-on technique described fully by Price et al. (2018), which makes use of the μL Nucleation by Immersed Particle Instrument (Whale et al., 2015). Filters were processed in a field laboratory set up in a hotel room to minimise the storage and transport effects that are known to lead to loss of INP (Beall et al., 2020). ~~Filters were typically processed within hours to a day after~~ All but one of the filters was processed within 24 h of collection. In these experiments, rectangular glass cover slips (48 mm x 64
130 mm, no. 1.5 thickness, *Agar Scientific, UK*) were washed with purified water (high performance liquid chromatography-grade, *Sigma-Aldrich, UK*) and isopropanol (*VWR, UK*) then immersed for 1 h in a petri dish containing Turtle Wax ClearVue Rain Repellent solution (*Rapid Electronics, UK*) to render them hydrophobic. The slides were removed from the ClearVue solution, rinsed with isopropanol and water, then dried with particle-free air from an oil-free air compressor (24 L, model HY7524, *Hyundai, UK*, with a HEPA filter in line). In a laminar flow hood, a filter onto which aerosol had been sampled was placed
135 onto a hydrophobic slide, and between 60 and 70 droplets of purified water with volume $2 \mu\text{L}$ were pipetted directly on to the filter using a manual electronic pipette. The hydrophobic glass slide/filter assembly was then placed onto the cold plate of an *Asymptote* EF600 Stirling engine-based cold stage with a drop of silicone oil in-between to aid thermal contact. A flow of HEPA-filtered compressed air that had been passed through a drying column (*Drierite 26800, Sigma-Aldrich, UK*) was used to flush the volume above the droplets to prevent frost formation. The filter was then cooled at a rate of 1 K min^{-1}
140 until all droplets froze. The cooling was recorded by a camera and the temperature of the cold plate measured concurrently. Software, written in Python, was used to automatically detect freezing events and determine the temperature at which each droplet froze (Barr, 2023). The same procedure was used for handling blanks from the aircraft. In addition, filter blanks were run each day, consisting of purified water droplets pipetted onto new, unhandled filters to ensure that the procedure and equipment were operating correctly and without unacceptable contamination (or the system cleaned and procedures improved
145 until contamination levels were deemed acceptable).

An alternative assay technique is to wash aerosol material off the filters in a larger volume of deionised water and take microlitre droplets from this volume for freezing experiments (O'Sullivan et al., 2018). Given the relatively short collection time for aerosols on the filters, the drop-on technique was chosen because it utilises a greater fraction of aerosols collected during the sampling period (approximately 30 times more aerosol per droplet). This gives greater sensitivity to the relatively small fraction
150 of all aerosols that are able to nucleate ice (Sanchez-Marroquin et al., 2021). ~~Comparison Using filters collected in parallel, comparison between the wash-off and drop-on techniques with filters collected in parallel, in shows good agreement in the INP concentration range over which they overlap, shows good agreement in many cases Sanchez-Marroquin et al. (2021) ranges where the techniques overlap (Sanchez-Marroquin et al., 2021).~~ However, in one-third of the cases the wash-off technique produced lower INP concentrations that at temperatures above $T = -20^\circ\text{C}$, temperatures at which biological and biologically-
155 enhanced INPs are active (Sanchez-Marroquin et al., 2021). The wash-off technique agrees well with other online and offline INP analysis techniques for mineral dusts (DeMott et al., 2018) but produced lower INP concentrations for a cellulose sample compared to other techniques (Hiranuma et al., 2019). Similarly, the wash-off technique has produced lower INP concentrations

than a liquid impinger technique when measuring INP in the Arctic, which was attributed to the larger size cut-off of the impinger technique (Li et al., 2023).

160 From droplet freezing temperatures, INP temperature spectra were derived using the framework of Vali (1971, 2019). For each assay, freezing events were grouped into temperature bins of size $\Delta T = 1$ K to calculate the differential nucleus spectrum,

$$k_{\text{assay}}(T) = -\frac{1}{V_d \Delta T} \ln \left(1 - \frac{\Delta N}{n(T)} \right), \quad (1)$$

where V_d is the droplet volume (2 μL), ΔN is the number of droplets that freeze in a temperature interval and $n(T)$ is the
165 number of droplets unfrozen at T , the upper limit of the bin's temperature range. The error on ΔN according to the Poisson distribution was propagated to find the error on $k_{\text{assay}}(T)$ for the individual spectrum. The average differential INP spectrum of the background filters, k_{bg} , was subtracted from the spectra for an individual assay to get the 'true' differential INP spectrum for a sample,

$$k(T) = k_{\text{assay}}(T) - k_{\text{bg}}(T). \quad (2)$$

170 From this, the INP concentration, N_{INP} , was calculated as

$$N_{\text{INP}}(T) = \frac{V_d A_f}{V_a A_d} \Delta T \sum_0^T k(T), \quad (3)$$

where V_a is the volume of air sampled, A_f is the surface area of the filter exposed to aerosol(11, (11 ± 2) cm²), and A_d is the surface area of the filter in contact with a droplet(0.01357, (0.014 ± 0.002) cm²). ~~A_f and A_d were calculated using spherical cap geometry with a contact angle of 126° as in Price et al. (2018).~~

175 2.3 Scanning electron microscopy

Using the method described by Sanchez-Marroquin et al. (2019), SEM-EDS was used on two filters to ascertain the size-resolved elemental composition of aerosol captured on the polycarbonate filters. The elemental ~~composition~~ composition was used to estimate the fraction of aerosol from terrestrial dust and marine sources. Portions of ~~filter~~ the filters were mounted on 25 ~~mm diameter stubs~~ and mm diameter stubs, sputter-coated with 30 nm of platinum and analysed at the University of Leeds with
180 a *Tescan Vega3 XM* electron microscope fitted with an *Oxford Instruments X-max 150 SSD* energy-dispersive X-ray spectrometer. Using *AZtec 3.3* feature recognition software, the filters were scanned for aerosol particles, and a prescribed algorithm was used to automatically classify particles into ~~types~~ categories (e.g. mineral dust and sea-spray) using their elemental composition. This classification algorithm is further described in Sanchez-Marroquin et al. (2019). The ~~classified particles were then binned according to their equivalent spherical diameter. A minimum diameter of 0.3 was chosen as it is comfortably above~~
185 ~~the size threshold at which the feature recognition software detects erroneously features. Using the total area of filter analysed by the SEM multiplied by the air volume sampled through it during the sampling run, it is then possible to calculate total surface area of aerosol of a certain composition, for example mineral dust or sea-spray aerosol.~~ The carbonaceous category of

particles includes those which contain no elements other than those O and C, and therefore does not distinguish between organic or elemental carbon. Biological particles are therefore not explicitly classified using this method but can be qualitatively identified on the basis on size and morphology (Sanchez-Marroquin et al., 2021). The classified particles were then binned according to their equivalent spherical diameter. A minimum diameter of 0.3 μm was chosen as it is comfortably above the size threshold at which the feature recognition software detects erroneously features. The total surface area of aerosol sampled in each composition category was normalised by the fraction of filter area analysed and the volume of air sampled during the sampling run.

195 2.4 Optical probes

Two under-wing optical probes were used to measure aerosol number, surface area and volume concentrations during the flight. These were the Passive Cavity Aerosol Spectrometer Probe 100-X (PCASP, *Droplet Measurement Technologies* with SPP200 electronics) and Cloud Droplet Probe (CDP, *Droplet Measurement Technologies*). Both probes operate by measuring the intensity of radiation from a laser that is scattered by incident particles. For the CDP, sampled particles pass directly through the beam, while for the PCASP, a sample is enclosed in clean air before entering an optical chamber. Both probes use the magnitude of the scattered radiation to assign the particle to one of 30 bins associated with the diameter of the particle (Rosenberg et al., 2012). Although the CDP is designed to measure droplets, it has previously been used to measure coarse-mode aerosol by adjusting the calibration of the probe to assume a refractive index representative of the aerosol sampled (Sanchez-Marroquin et al., 2020). To do this, the calibration method of Rosenberg et al. (2012) was used to calculate the particle diameters measured by each bin when given a refractive index. For this study, particle size distributions were first obtained using real refractive indices ranging from 1.5–1.7 and imaginary components from 0–0.003i as in Sanchez-Marroquin et al. (2020). Since the error associated with refractive index was small, a refractive index value of $1.56 + 0i$ was chosen for consistency with Sanchez-Marroquin et al. (2020). When using a refractive index of 1.56, the PCASP measures particles with a diameter range of 0.1–3 μm , while the CDP measures particles with a diameter range of 4.5–70 μm .

210 Previous studies have found that the ~~INP filter system may enhance coarse-mode aerosol number relative to measurements made by the PCASP-CDP probe (Sanchez-Marroquin et al., 2019; Barr, 2023). This discrepancy was minimised by fully opening the bypass line open as recommended by Sanchez-Marroquin et al. (2019). In addition, use of the coarse mode aerosol number reported by the PCASP and CDP probes is suppressed relative to particles counted on filter samples using SEM (Sanchez-Marroquin et al., 2019; Barr, 2023). The use of~~ larger pore filters ~~results in a greater sample flow which further reduces sub-isokinetic sampling biases; and a fully-open bypass line (as described in Sect. 2.2) minimised this discrepancy.~~

215 To ensure that no cloud droplets or swollen hygroscopic aerosol were reported by the CDP, CDP data ~~has~~ have only been used when relative humidity was below 80% and when cloud-free air was identified using the Nevzorov hot-wire instrument. The Nevzorov instrument derives the liquid and total condensed water content (liquid and ice) based on the power required to melt and evaporate hydrometeors collected by the instrument (Korolev et al., 1998; Abel et al., 2014). The power supplied to the Nevzorov probe is significantly different in- and out-of-cloud. Using this variation in power supply, a 1 Hz cloud-flag was derived to partition the data as in- or out-of-cloud in a similar manner to Barrett et al. (2020).

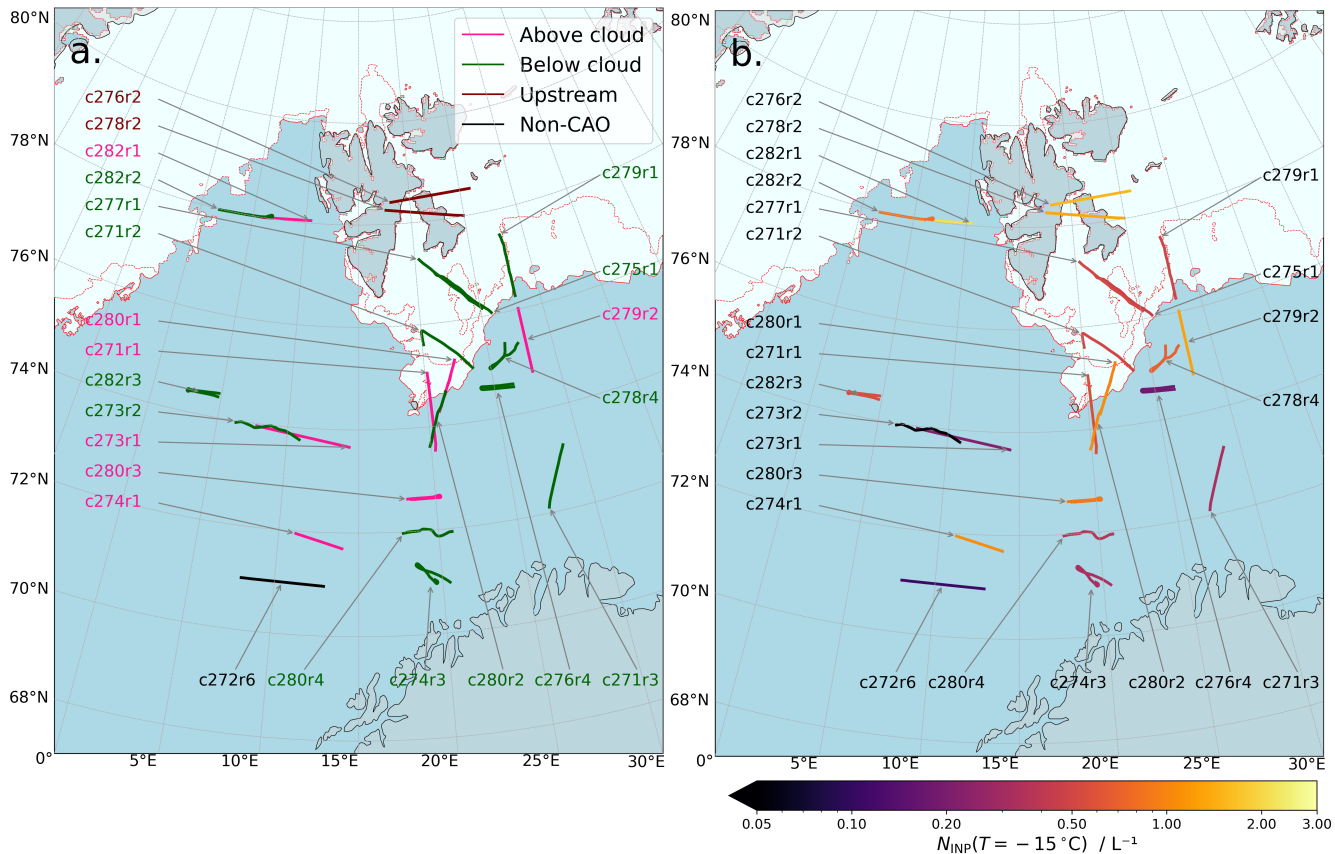


Figure 2. Locations of all filter samples taken during the ACAO campaign. Panel **a** displays the location of the sample relative to the cloud deck while panel **b** shows $N_{\text{INP}}(-15^\circ\text{C})$, the temperature at which an INP concentration of 0.5 was measured at -15°C for each sample. All filters were taken in CAO conditions except ~~e272r6~~ c272r6.

3 Results

Successful INP analysis was performed on 23 filter samples. All but filter ~~e272r6~~ c272r6 were taken when mixed-phase boundary layer clouds associated with cold-air outbreaks were present. 13 samples were taken above the cloud deck, eight
 225 were taken below the cloud deck and two were taken upstream of the development of the cloud in clear air. These sampling locations were considered to represent air below, above and before the development of the atmospheric boundary layer over sea respectively. The locations, altitudes and purpose of each filter measurement is shown in Table 1. Figure 2a shows that the filter tracks were distributed throughout the development of the cold-air outbreaks.

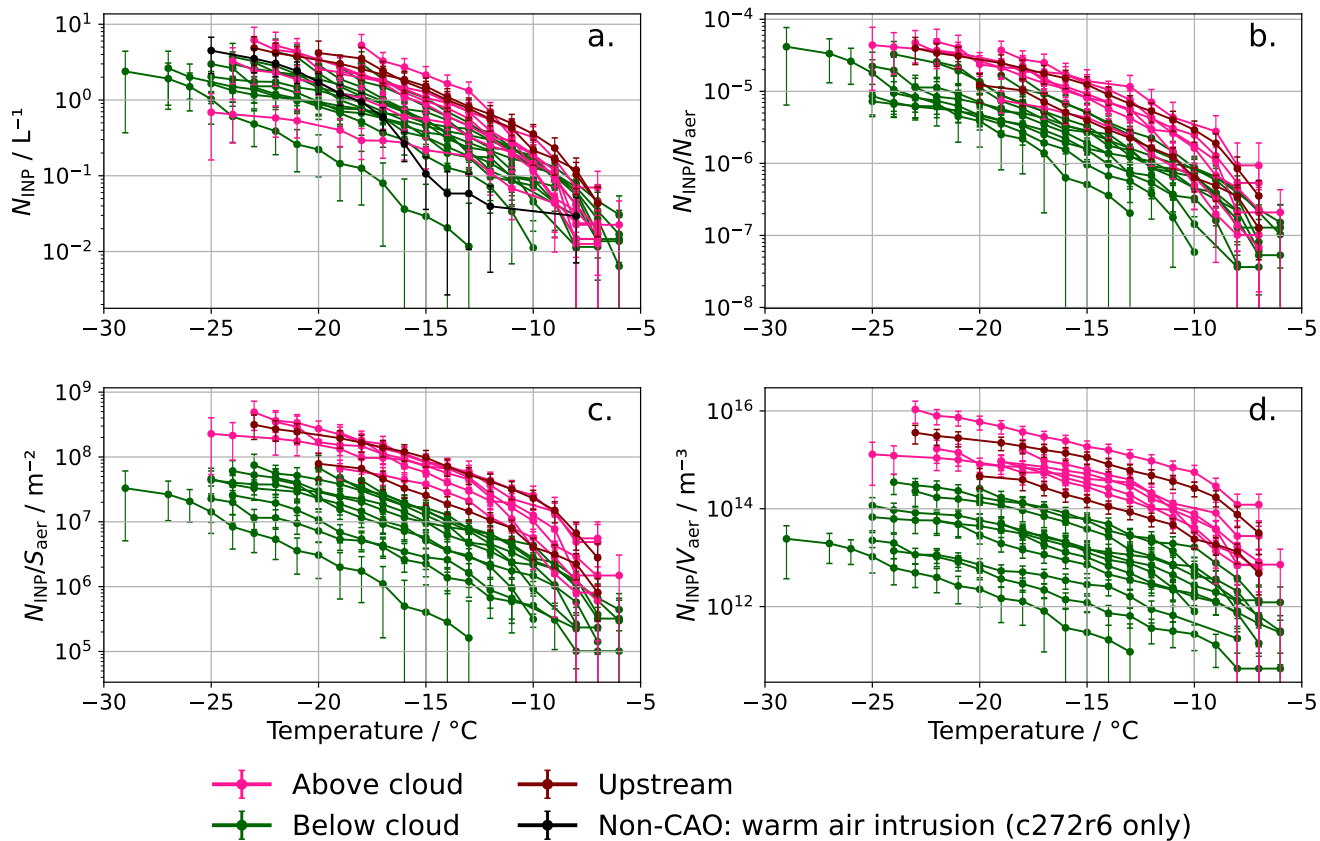


Figure 3. Panel **a** shows INP concentrations for each sample made during the campaign. Panels **b**, **c** and **d** show these concentrations normalised by the total number (N_{aer}), surface area (S_{aer}) and volume (V_{aer}) of aerosols with diameters greater than $0.1 \mu\text{m}$. Colours and symbols A version of samples are consistent throughout all panels this figure where each sample is individually labelled can be found in Appendix A.

3.1 INP concentration spectra

230 Figure 3a shows a composite of the INP concentration spectra ($N_{\text{INP}}(T)$) measured throughout the campaign. Measurements on and after the 21st March (e274 c274 onwards, when the flows had a northerly component) form a tight band of INP spectra, all falling within about one order of magnitude and centred at about 1 L^{-1} at $-15 \text{ }^\circ\text{C}$. Spectra from the 11th March through to the 19th March (flights c271 to c273), when the flow directions were from the west or south had much more variable INP concentrations with one filter measurement recording an INP concentration below 0.1 L^{-1} at $-15 \text{ }^\circ\text{C}$ (e273r2)-c273r2) (see Fig A1). The median CAO INP concentration during the campaign, \bar{N}_{INP} , was described by the function

$$\bar{N}_{\text{INP}} = \bar{\nu}_{\text{INP}} \exp \left[\bar{a} (\bar{T}_{\text{max}} - T)^{\bar{b}} \right], \quad (4)$$

with fitting parameters $\bar{\nu}_{\text{INP}} = 1.480 \times 10^{-2} \text{ L}^{-1}$, $\bar{T}_{\text{max}} = 226.2 \text{ K}$, $\bar{a} = 1.271 \text{ K}^{-0.5}$ and $\bar{b} = 0.5$. The fitting procedure used to obtain \bar{N}_{INP} is described in Appendix B, along with similar four-parameter fits for each individual filter measurement. Figure 4 shows that INP concentrations during the ACAO campaign were among the highest recorded in the high latitudes of the Northern Hemisphere in springtime. They are comparable with the highest mid-latitude INP measurements collated by Petters and Wright (2015) and INP concentrations measured by Sanchez-Marroquin et al. (2020) in autumnal Icelandic dust plumes. They were also similar to the highest INP concentrations reported by Porter et al. (2022) at the North Pole in August 2018 when aerosol was transported from the Russian coast. Both Rogers et al. (2001) and Prenni et al. (2007) used an online thermal gradient diffusion chamber to quantify INP from an aircraft north of Alaska during May and September-October, respectively. While they often saw no detectable INPs, they also report periods when INP concentrations were comparable to (or sometimes greater than) those found in ACAO. Sanchez-Marroquin et al. (2023) report airborne INP measurements from March in northern Alaska using the same filter technique as used in ACAO, revealing INP concentrations at least 1-2 orders lower than in ACAO, with a steeper slope (many measurements were consistent with the background). These flights were not focused on CAO events.

250 The only previous airborne springtime INP measurements made in vicinity of Svalbard were made by Hartmann et al. (2020), who flew over sea ice in the Arctic Ocean and Fram Strait in late March and early April 2018 and collected aerosol onto polycarbonate filters for a wash-off droplet freezing assay. Hartmann et al. (2020) collected filter samples from an entire flight rather than in specific locations and reported INP concentrations that were 1-2 orders of magnitude lower than observed during ACAO in three out of nine samples. The other six samples had lower INP concentrations, often consistent with their handling blanks. The three higher INP samples, which contained heat sensitive INP, were associated with airflows with a strong northerly component and satellite imagery (MODIS Land Science Team, 2020) shows classic CAOs on these days. In contrast, the other samples were associated with less well-defined air mass trajectories that were not CAO events or, in one case, a CAO where the air originated from the west in the Canadian archipelago rather than the central Arctic.

260 Geerts et al. (2022) reported INP concentrations derived using the wash-off technique during CAOs from December 2019 to May 2020 at Andenes on the coast of northern Norway. The ground based measurements at this downstream site revealed INP concentrations that were 2–3 orders of magnitude lower than in ACAO. This might be consistent with loss of INP in

the precipitating clouds in the CAO. Ground measurements of INP concentrations made during 2012 by Wex et al. (2019) in Ny-Ålesund (upstream of the CAO clouds in ACAO), using a quartz filter technique, were also 2–3 orders of magnitude lower than those observed during ACAO. However, the highest INP concentrations observed in this dataset occurred during the summer, rather than the springtime. A similar seasonal dependence was also observed in the high Arctic by Creamean et al. (2022), who observed INP concentrations 2–4 orders of magnitude below those in the ACAO campaign during their year-round INP measurements. Creamean et al. (2022) used a technique that involved size selecting aerosol and impacting them onto petrolatum and then recovering these particles into water for a droplet freezing assay. Ship-based measurements of INP in the ocean around Svalbard ~~made-~~, made with the wash-off technique between May and July 2017, ~~made with the wash-off technique-~~, were 1–2 orders of magnitude below those made during the ACAO campaign (Hartmann et al., 2021).

Rinaldi et al. (2021) used two offline methods to measure INP concentrations sampled at a ground-based site near Ny-Ålesund between April and August 2018. They found that using a Dynamics Filter Processing Chamber to measure INP concentration using condensation freezing yielded INP concentrations approximately eight times greater than those yielded by a droplet-freezing assay measurement using a wash-off technique. However, the highest concentrations measured by Rinaldi et al. (2021) were lower than the lowest observed during ACAO and were typically 1–3 orders of magnitude below those made during the ACAO campaign (Hartmann et al., 2021) measured in this campaign. Similarly, Li et al. (2023) used several different techniques to measure INP at a Ny-Ålesund ground site during October and November 2019. These included an impinger sampling method, a continuous flow diffusion chamber (CFDC) and a polycarbonate filter wash-off technique. These measurements had a much greater spread than those in ACAO and were typically 1–4 orders of magnitude lower. However, the measurement spread reduced at lower temperatures, and if extrapolated log-linearly, wash-off measurements were consistent with measurements made by the CFDC at $T = -30$ °C. Similarly, although the CFDC measurements were made at lower temperatures than INP measurements in ACAO, the two were consistent if the ACAO spectra were extrapolated log-linearly as the gradient of INP spectra in ACAO was lower than those measured by Li et al. (2023).

Comparison with the INP literature presents a somewhat confusing picture. It may simply be the case that there is strong variability on a range of ~~spaeial~~-spatial and temporal scales. However, there may also be differences between techniques. As noted in the methods section, intercomparison of assay techniques reveals similar results for some INP types (DeMott et al., 2018; Wex et al., 2019), but substantial differences between different techniques for some INP types (Hiranuma et al., 2019). ~~(Beall et al., 2020) Additionally, intercomparison of assay techniques on simultaneously-taken samples of ambient aerosol during field campaigns has shown both consistencies and inconsistencies between techniques (Li et al., 2023; Lacher et al., 2024)~~. Beall et al. (2020) report that biological INP can sometimes be lost on storage and transport, which we largely avoid by processing our filters during the campaign in a temporary laboratory. While the droplet-on-filter technique used here was not included in the formal intercomparisons, it has shown different responses in other environments and the results are consistent with what might be expected. For example, this technique produced INP concentrations several orders of magnitude smaller than in ACAO during March 2018 near Alaska (Sanchez-Marroquin et al., 2023). In dust plums-plumes emerging from Africa, this technique produced much steeper INP spectra than in ACAO (Price et al., 2018) and the INP concentrations were consistent with laboratory derived activity of K-feldspar in mineral dust (Harrison et al., 2019). Measurements in the UK revealed a strong

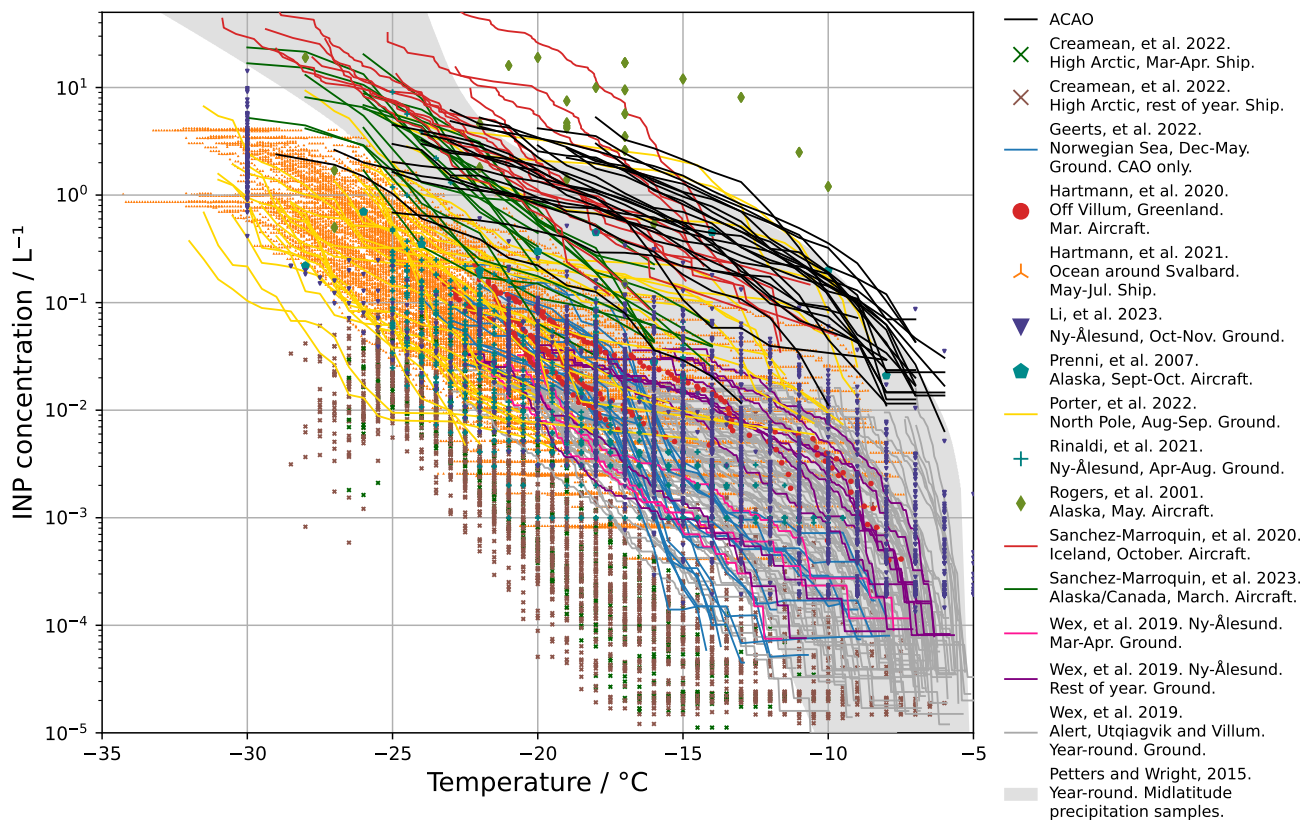


Figure 4. INP concentrations measured in a number of different field campaigns in the Arctic (Creamean et al., 2022; Geerts et al., 2022; Hartmann et al., 2020, 2021; Porter et al., 2022; Sanchez-Marroquin et al., 2020, 2023; Wex et al., 2019) (Creamean et al., 2022; Geerts et al., 2022; Hartmann et al., 2020, 2021; Li et al., 2023; Prenni et al., 2007; Porter et al., 2022; Rogers et al., 2001; Rinaldi et al., 2021). These are compared to mid-latitude INP measurements from precipitation samples collated by Petters and Wright (2015).

biological ‘hump’ consistent with ground-based measurements (Sanchez-Marroquin et al., 2021). In addition, measurements in dust plumes emerging from Iceland produced active site densities consistent with laboratory measurements of Icelandic dust (Sanchez-Marroquin et al., 2020) and other high latitude dusts (Barr et al., 2023). Continued efforts are needed to intercompare
 300 INP assay techniques and better understand the influence of storage, but high Arctic INP concentrations have been observed using various techniques by various groups.

Overall, the literature in combination with our new measurements indicates that INP concentrations during northerly CAOs in this region, where the air is drawn from the central Arctic, can at least sometimes have mid-latitude like INP concentrations.

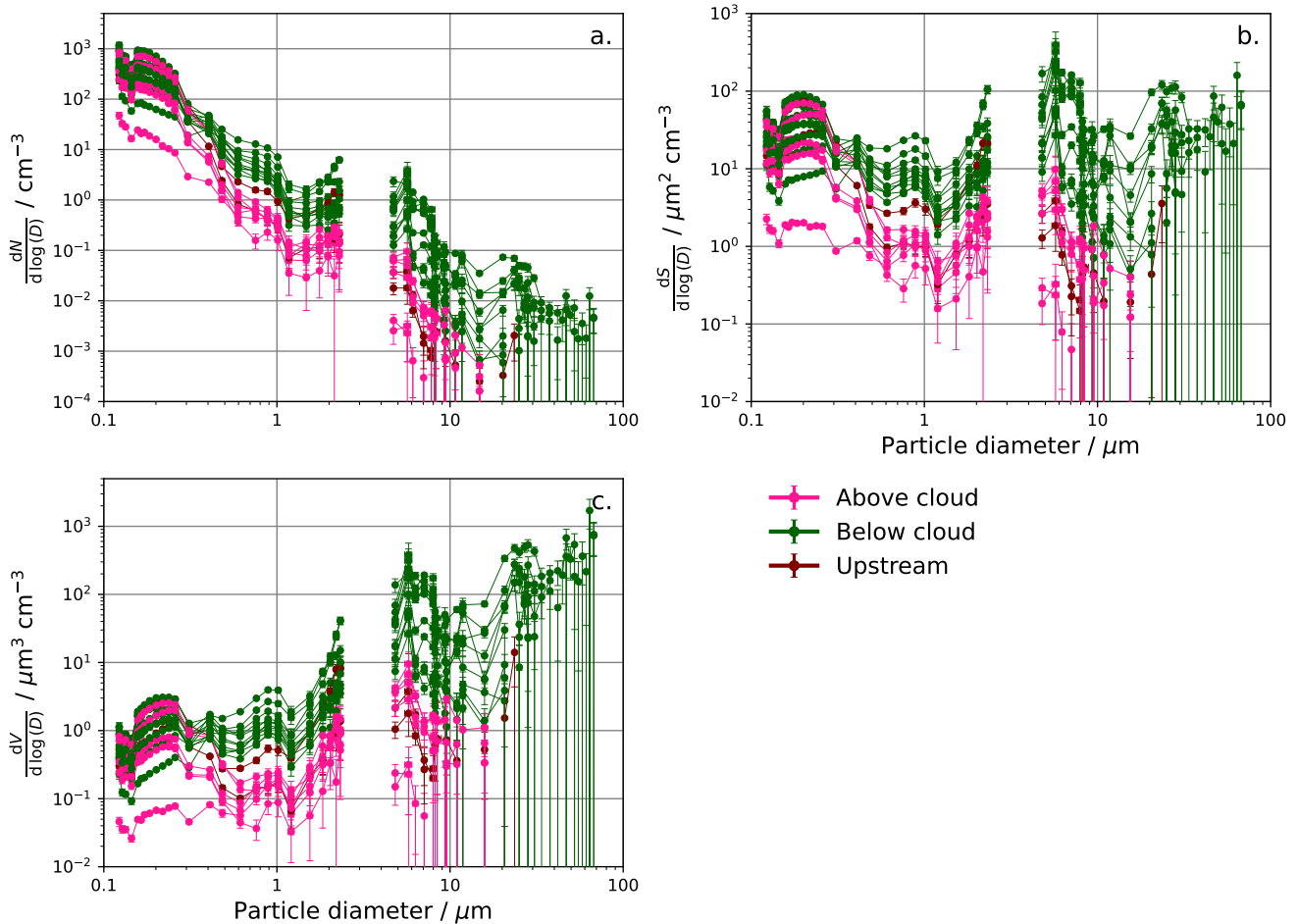


Figure 5. Size distributions of **a** particle number, **b** particle surface area and **c** particle volume measured with the PCASP and CDP probes during each filter sample. Probe data was unavailable during flights [e271](#) [c271](#) and [e272](#) [c272](#). [A version of this figure where each size distribution is individually labelled according to the sample it is associated with can be found in Appendix A.](#)

3.2 Aerosol environment in CAOs

305 To try to understand the sources and variation of the high INP concentrations observed during the campaign, we used observations from the PCASP and CDP underwing probes to investigate the aerosol environments during filter sampling.

Size distributions of aerosol particle number, N , surface area, S , and volume, V , are presented in [Figures Figure 5](#). To derive surface area and volume, aerosols were assumed to be spherical. The size distributions of aerosol measured during the campaign were mostly similar in shape, but with values of $dN/d\log(D)$ that spanned 2 orders of magnitude. Number
 310 concentrations of aerosol were dominated by sub-micron particles. Few super-coarse aerosol particles (diameter $D > 10 \mu\text{m}$) were observed, though particles with diameters greater than $30 \mu\text{m}$ were at the edge of the detection ability of the CDP. Sub-

and super-micron particles contributed approximately equally to the total surface area of the aerosol. Number concentrations of aerosol observed were consistent with those observed over the Norwegian Sea during the March–April 2013 Aerosol-Cloud Coupling And Climate Interactions in the Arctic (ACCACIA) aircraft campaign using the PCASP and CDP instruments by (Young et al., 2016) [Young et al. \(2016\)](#). However, the number concentration of sub-micron aerosol was up to 2 orders of magnitude greater than in March observations of aerosol using a ground-based aerodynamic particle sizer near to Ny-Ålesund made by Song et al. (2021) from 2015–2019. [The number concentration of aerosol with diameter between 0.1–0.5 μm observed during ACAO was also an order of magnitude greater than that measured at Ny-Ålesund during the COMBLE campaign, though concentrations were similar between 0.5–1 μm \(Williams et al., 2024\).](#)

Figure 6 shows aerosol profiles from each of the flights where PCASP and CDP data ~~was~~ [were](#) available. Measurements of aerosol concentration where ~~INP concentration~~ filter samples were made are highlighted ~~in orange~~ [according to their INP concentration](#), showing that the INP filter samples taken were subject to in aerosol concentrations representative of the aerosol environment at these heights measured throughout the flight. Aerosol concentrations near the sea-surface (<500 m above sea level) were consistently 100–200 cm⁻³. These measurements were comparable to measurements made in early April 2022 near Svalbard during the HALO-AC³ campaign (Wendisch et al., 2024). However, the vertical distribution of aerosol varied much more between flight days. On three flying days (~~e274, e277/e278 and e281/e282~~), aerosol concentrations were approximately constant [from the surface up to 7500 m](#). These ~~were c274, which had a northwesterly flow, and c277/c278 and c281/c282, which both had northerly flows. These~~ contrasted with three days where the aerosol concentration decreased with altitude in the boundary layer (~~e273, e275/e276 and e279~~) ~~and one day where~~. [These were c273, which had a westerly flow, and c275/c276 and c279, which both had northerly flows. Finally,](#) aerosol concentrations increased with altitude ~~e280~~ [during flight c280, another day with a northerly flow.](#)

3.3 Size-resolved aerosol composition

SEM analysis to determine size resolved composition was performed on two polycarbonate filters sampled during filter runs ~~e279r1 and e278r2~~ [c279r1 and c278r2](#). These filters were selected to represent the aerosol upstream of the CAOs. ~~Filter e279r1~~, and had $N_{\text{INP}}(-15^{\circ}\text{C})$ of $(0.49 \pm 0.15) \text{ L}^{-1}$ and $(1.4 \pm 0.4) \text{ L}^{-1}$ respectively. [These represent INP concentrations at the 33rd and 90th percentiles of samples taken in CAOs. Filter c279r1](#) was sampled at an altitude of 155 m over the marginal sea ice zone, while filter ~~e278r2~~ [c278r2](#) was sampled at an altitude of 1725 m above the Svalbard archipelago and surrounding sea ice, prior to cloud development. The size and elemental proportions of 1,101 and 451 particles respectively were analysed on these filters.

Composition analysis and particle-size distributions [derived using SEM](#) for each of the filters are shown in Figure 7. [Figure 7 also compares the particle-size distributions derived using SEM with those derived from the PCASP and CDP.](#) Both filters showed that a large proportion of the particles were consistent with mineral dusts, with Si-rich and Al/Si-rich particles representing over half of the proportion of super-micron particles. There were also significant numbers of carbonaceous aerosol in the sub-micron range, although ~~our~~ [this](#) method cannot confirm if they were of biological origin. We did not note any particles that were qualitatively of biological origin on the basis of size or morphology, as ~~we have done previously~~

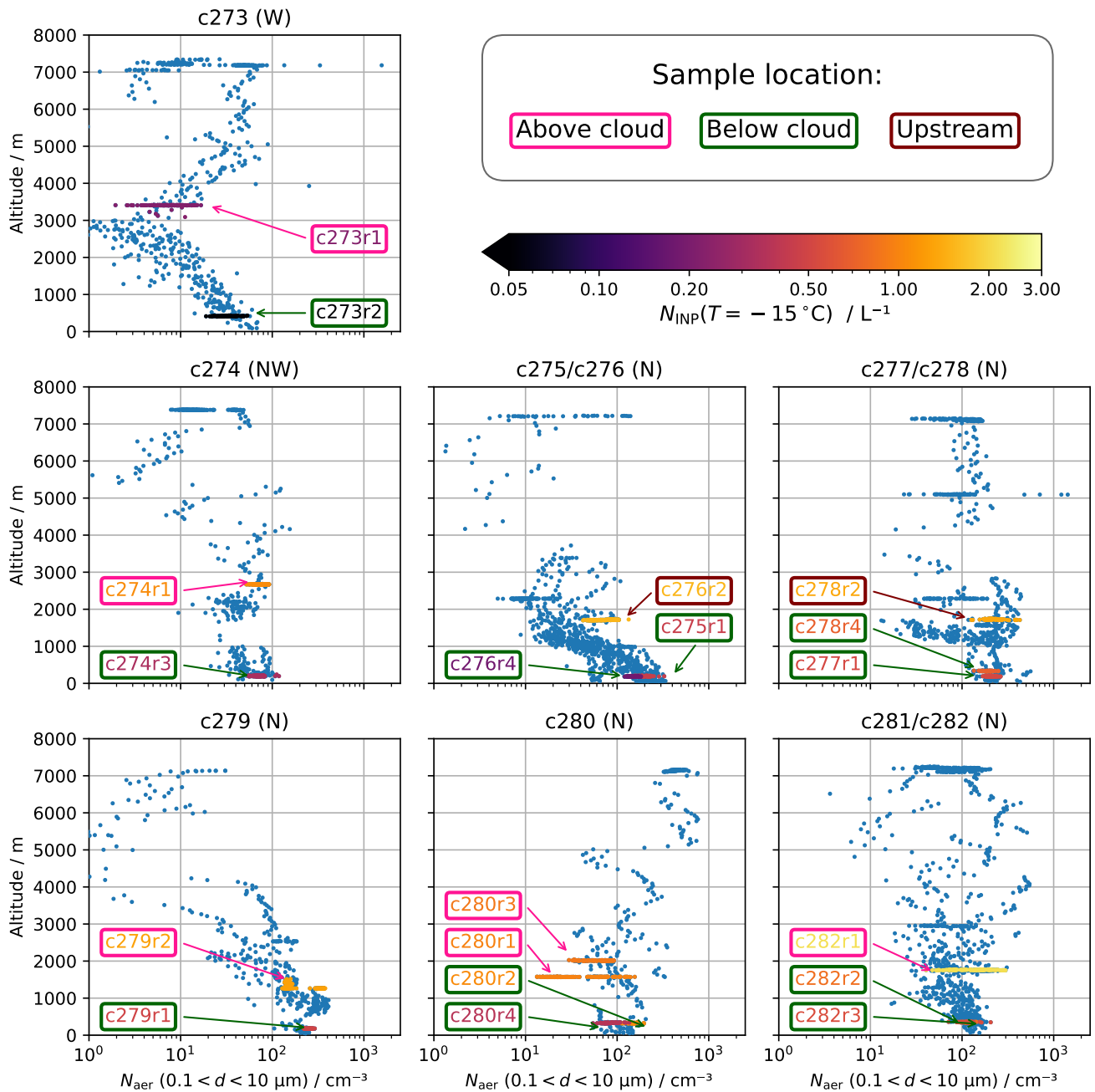


Figure 6. Out-of-cloud aerosol measurements made using the PCASP and CDP averaged every ten seconds. Measurements made during filter sampling are highlighted in orange coloured and labelled according to their INP concentration at $T = -15\text{ °C}$. The borders of each label and the arrows matching labels to measurements are coloured according to the location of the sample relative to the CAO cloud. Measurements over or close to land and the Scandinavian Peninsula were discarded to represent Arctic and oceanic air only.

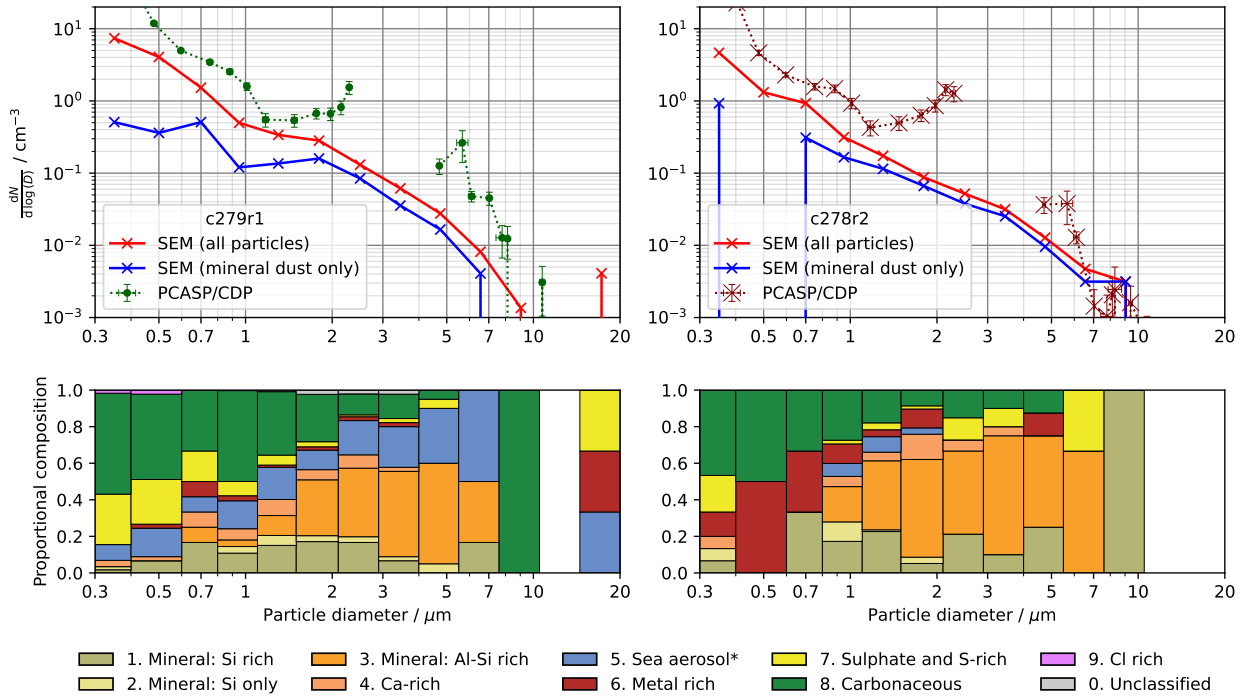


Figure 7. Particle-size distributions and particle composition derived from scanning electron microscopy for filters ~~e279r1~~ c279r1 (left) and ~~e278r2~~ c278r2 (right). Sample c278r2 was taken upstream of cloud development, while sample c279r1 was taken below the northern extent of CAO cloud streets. Both were taken in northerly CAOs. Solid lines show particle-size distributions derived directly from the SEM measurements, while dotted lines show the particle-size distribution derived from the underwing probes in the diameter ranges, as in Fig. 5. Composition is shown for each size bin. Size bins with greater values of $dN/d\log(D)$ contain more particles. White regions of the composition plots indicate that no particles were detected in this size range. Sea aerosol refers to aerosols likely to correspond to either fresh, aged or mixed sea spray aerosols.

(~~Sanchez-Marroquin et al., 2021~~), noted previously in Sanchez-Marroquin et al. (2021). However, due to the relatively small fraction of filter analysed, their presence cannot be ruled out. Despite filter sample ~~e278r2~~ c279r1 being taken close to the marginal ice surface, less than a quarter of the particles showed clear signatures of sea-spray (such as the presence of both sodium and chlorine), though some of the carbonaceous or sulfurous aerosol could be of marine origin. The total surface area of mineral dust particles, being the sum of Si-rich, Si-Al rich, Si only and Ca-rich classes, was calculated as $1.0 \mu\text{m}^2\text{cm}^{-3}$ and $0.6 \mu\text{m}^2\text{cm}^{-3}$ for ~~e279r1~~ and e278r2 c279r1 and c278r2, respectively. These values are consistent with measurements of aerosol 91 – 375 m over the Norwegian Sea in March by Young et al. (2016) made during the ACCACIA campaign. Filter ~~e279r1~~ c279r1 showed very few particles with clear sea-spray signatures, consistent with its higher altitude and location over sea ice. Metal-rich particles are present in the smaller size fraction, although these have been previously found as contaminant

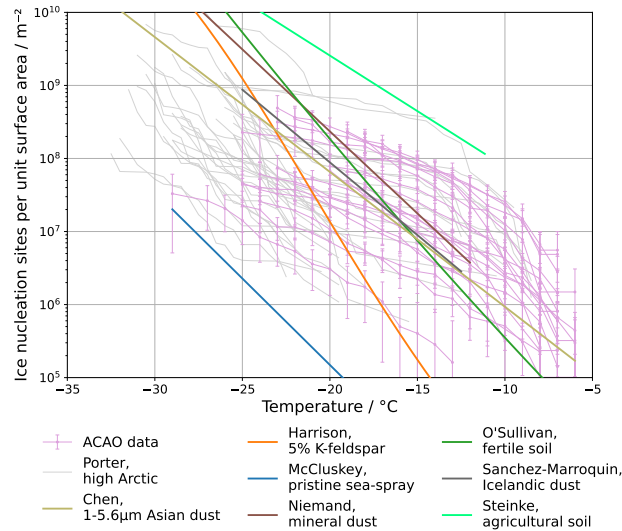


Figure 8. A comparison of $N_{\text{INP}}/S_{\text{aer}}$ measured during the ACAO campaign to measurements of active ice nucleation site density in the high Arctic by Porter et al. (2022) and parametrisations of active ice nucleation site density (Chen et al., 2021; Harrison et al., 2019; McCluskey et al., 2018b; Niemand et al., 2012; O’Sullivan et al., 2018; Sanchez-Marroquin et al., 2020; Steinke et al., 2016).

355 particles on blank filters. These were likely to be produced by the microscope mechanism so it is not clear if they are artefacts or from the atmosphere.

The aerosol number measured by the SEM is generally 2–4 times below the aerosol number reported by the PCASP and CDP probes, or shifted to about 30% smaller sizes. Previous studies using this technique have also found similar magnitudes of discrepancy between the techniques. In these cases, SEM has sometimes measured more particles than the optical probes, and sometimes less (Sanchez-Marroquin et al., 2020, 2021). Using a different SEM technique, Young et al. (2016) found the PCASP and CDP probes reported concentrations up to 100 times greater than SEM and attributed this larger discrepancy to measurements of cloud droplets or swollen aerosol since they sampled at high relative humidity (RH), often with $\text{RH} > 90\%$. We discarded PCASP measurements made in-cloud or above $\text{RH} = 80\%$ to bias against swollen aerosol. However, even at $\text{RH} = 80\%$, the diameter growth factor of typical organic aerosol has been reported between 20–50% (Martin et al., 2003; Latimer and Martin 2003). For sea salt, the diameter growth factor at $\text{RH} = 80\%$ has been reported between 60–100% (Tang et al., 1997; Martin et al., 2003; Murray et al., 2005). Hygroscopic growth of these species might go some way to explaining our discrepancy. However, the measured size and number of the mineral dust particles should not be affected by humidity.

3.4 Ice-nucleating activity of samples

To determine how ice-nucleating activity depends on the physical properties of the aerosols, the aerosol-size distributions presented in Figure 5 were used to calculate total aerosol number N_{aer} , surface area, S_{aer} , and volume, V_{aer} for aerosols with $D > 0.1 \mu\text{m}$, assuming spherical geometry. Figure 3 shows the INP concentrations normalised by aerosol number, area and

volume. Normalising N_{INP} by N_{aer} failed to reduce the spread in values between measurements, while normalising by S_{aer} and V_{aer} increased the spread between measurements. This indicates that the INP concentration does not scale with the overall aerosol surface area or volume. This is consistent with the INP being a subset of the aerosol particle population with non-ice nucleating components of the aerosol particle population being the primary driver of variability in S_{aer} and V_{aer} . [Other studies of Arctic and high-latitude INP \(e.g. Porter et al. \(2022\); Barr et al. \(2023\); Sanchez-Marroquin et al. \(2023\); Moore et al. \(2024\)\) have also found that normalising by surface area fails to reduce the measurement spread.](#)

In Figure 8, measurements of $N_{\text{INP}}/S_{\text{aer}}$ are compared to measurements of active site density reported for well-defined samples as well as from other field campaigns. Both the magnitude and shape of the curve of $N_{\text{INP}}/S_{\text{aer}}$ values from ACAO are similar to those measured by Porter et al. (2022) at the North Pole in late summer. This indicates that there is perhaps some commonality in INP between these two campaigns, even though the timing and location were very different.

To compare $N_{\text{INP}}/S_{\text{aer}}$ to active site density for well-defined samples, such as mineral dusts or sea spray, we note that these comprise only a fraction of the surface area in the aerosol samples in ACAO (see Figure 7). In the case of sea spray, our $N_{\text{INP}}/S_{\text{aer}}$ values are many orders of magnitude greater than the active site density for pristine sea spray reported by McCluskey et al. (2018b), hence we conclude that the INPs we observe are not related to pristine sea spray.

Integration of the size distributions in Figure 7 reveals that 32% ($e279p1c279p1$) and 53% ($e278p2c278p2$) of the overall aerosol surface area was mineral dust. Assuming that the aerosol composition was similar across the campaign, values of $N_{\text{INP}}/S_{\text{aer}}$ would be 2–3 times smaller than values of active site density normalised to the mineral dust surface area rather than the overall aerosol surface area. This allows us to compare with literature parametrisations of active site density for minerals in mineral dust, desert dusts and soil dusts containing ice-active organic material in Figure 8. Comparison with K-feldspar, the most active mineral component of atmospheric mineral dusts (Harrison et al., 2019; Vergara-Temprado et al., 2017) shows that K-feldspar alone cannot account for the magnitude of the observed active site densities above $-20\text{ }^{\circ}\text{C}$ as the temperature dependence is too steep. This implies that there is some other component in these samples that nucleate ice. Above $-20\text{ }^{\circ}\text{C}$, measurements fall between the active site densities reported for agricultural soil by Steinke et al. (2016), fertile soils by O’Sullivan et al. (2018) and general mineral dusts (from fertile and infertile sources) by Niemand et al. (2012). The measurements are also similar to the active site densities for super-micron Asian dust reported by Chen et al. (2021) and Icelandic dust measured by Sanchez-Marroquin et al. (2020).

In conclusion, the high values of $N_{\text{INP}}/S_{\text{aer}}$ of the ACAO samples at temperatures greater than $-20\text{ }^{\circ}\text{C}$ suggests a strong biogenic component to the INP population (Huang et al., 2021), potentially corresponding to mineral dust containing biological components, such as fertile soils.

3.5 INP spectra curve fitting

~~All measured temperature spectra for (a) INP concentration and (b) INP concentration normalised by aerosol surface area were fitted to Eq. B1 and B2 respectively. In both panels, examples of fits to a high, medium and low spectrum are demonstrated. In panel a, the red line shows the function fitted to the median INP concentration observed during the campaign, where~~

405 $\nu_{\text{INP}} = 1.480 \times 10^{-2}$, $T_{\text{max}} = 266.2$, $a = 1.271 \text{ K}^{-b}$ and $b = 0.5$. In panel **b**, the red line shows the function fitted to the median active site density observed during the campaign, where $\nu_{\text{S}} = 3.501 \times 10^5$, $T_{\text{max}} = 266.4$, $a = 1.279 \text{ K}^{-b}$ and $b = 0.5$.

Our measurements show that the entire INP spectrum ($N_{\text{INP}}(T)$) varied over the campaign (Figure 3). To represent the INP concentration across the full temperature spectrum in future modelling work, we fitted all spectra to a four-parameter function. This function took the form

410
$$N_{\text{INP}} = \nu_{\text{INP}} \exp \left[a (T_{\text{max}} - T)^b \right],$$

The parameter T_{max} represents the greatest temperature at which a freezing event was observed, a and b are shape parameters that determine the curvature of the function, and ν_{INP} is a scale parameter related to INP concentrations (if the shape were constant). For INP spectra with the same shape, greater values of ν_{INP} indicate greater INP concentrations across the entire temperature range. The same functional form was also applied to active site density spectra, which were fitted to the equation

415
$$N_{\text{INP}} = \nu_{\text{S}} \exp \left[a (T_{\text{max}} - T)^b \right]$$

Fitting parameters for all spectra are given in Table B1, while examples of this fitting are shown in Figure B1, where functions for three individual samples, [e273r2](#), [e277r1](#) and [e276r2](#) are illustrated. These represent filter measurements with low, medium and high INP concentrations and active site densities and demonstrate the ability of the function to represent all INP concentrations during the campaign. Equations B1 and B2 were also used to create parametrisations for the median
 420 INP concentration and active site density across the campaign for spring-time CAOs in the region (excluding [e272r6](#), which was not made in cold-air outbreak conditions). These are also shown in Figure B1.

3.5 Variation in INP properties with altitude and position in CAOs

To understand how the INP spectra varied with altitude in northerly CAOs (flights [e274 to e282](#), [e274 to e282](#)), $N_{\text{INP}}(-15^\circ\text{C})$, the INP concentration at -15°C , as well as the same quantity normalised by surface area, is shown relative to altitude in Fig-
 425 ure 9. This temperature was chosen to be representative of typical cloud temperatures in ACAO and as spectra with relatively high INP concentrations at -15°C had similarly high concentrations relative to other INP spectra in the campaign across all temperatures.

Considering $N_{\text{INP}}(-15^\circ\text{C})$, the samples fall into two groups, [as shown in Figure 3](#). Samples taken above cloud and up-stream of the clouds fall into a group where mean $N_{\text{INP}}(-15^\circ\text{C}) = 1.3 \text{ L}^{-1}$ above the cloud, whereas the below-cloud value
 430 is 0.54 L^{-1} . This indicates that the below cloud INP concentrations are approximately 2.4 times smaller than the above-cloud measurements. This is consistent with a free tropospheric source of INP rather than a source from the surface. It is also possible that there is a removal of INP in clouds, which we return to below. When normalised to the aerosol surface area ($N_{\text{INP}}(-15^\circ\text{C})/S_{\text{aer}}$), the gap between the two groups is even larger with above cloud values ~~are approximately 7.0~~
[approximately 8.8](#) times larger than the below cloud values. [Similar relationships between INP activity and altitude were found](#)
 435 [by Moore et al. \(2024\) who observed INP concentrations normalised by surface area above cloud in the SOCRATES campaign](#)

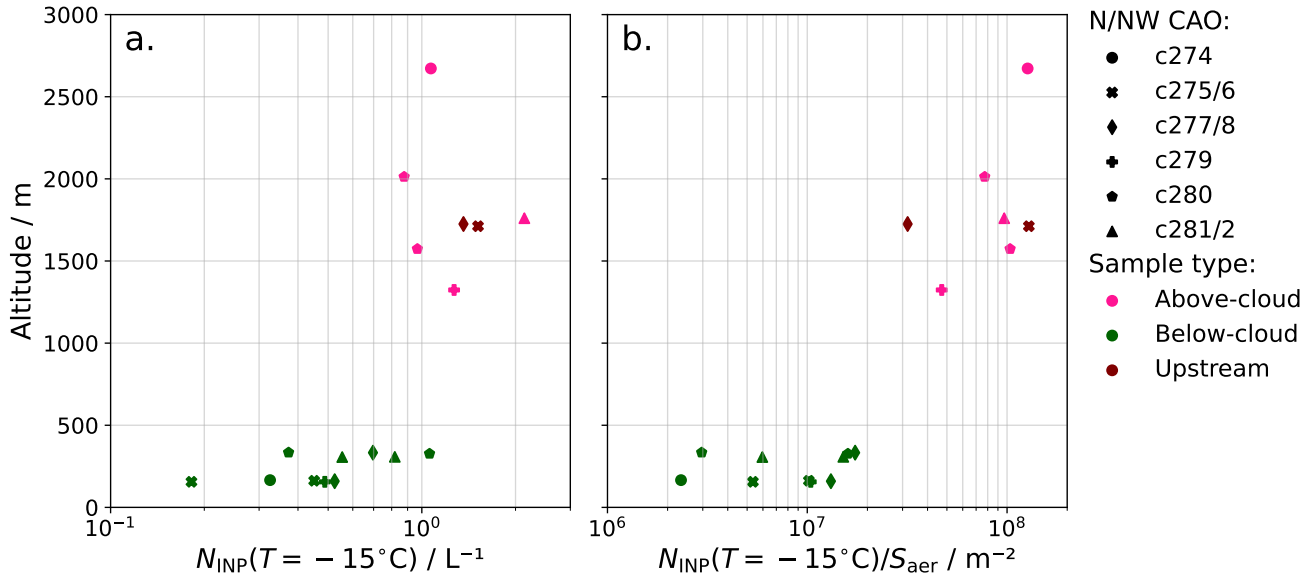


Figure 9. Variation with altitude of **a** INP concentration at -15°C and **b** INP concentration at -15°C normalised by aerosol surface area in northerly CAOs.

were greater than those below cloud. Additionally, Knopf et al. (2023) found that during measurements on INP in the Eastern North Atlantic, the efficiency of deposition ice nucleation was greater for samples taken in the free troposphere than the marine boundary layer. The reduced $N_{\text{INP}}(-15^{\circ}\text{C})/S_{\text{aer}}$ below cloud is due to the enhanced aerosol surface area below cloud in the CAO that was most likely related to the enhanced sea spray production (consistent with the visual observations of extreme sea states related to the high wind speeds in the CAOs that we flew in). The enhanced aerosol surface area below cloud compared to above cloud is clear from Figure 5. This reduction in activity is consistent with the sea spray producing a negligible concentration of INPs (see section 3.4), but where this additional aerosol reduces the active site density. Using the average below-cloud aerosol surface area with the parametrisation of (McCluskey et al., 2018b), the INP concentration at -15°C would be expected to be 7×10^{-4} ~~4×10^{-4}~~ L^{-1} if the only INPs below cloud were sea-spray. Our measured INP concentration is more than 3 orders of magnitude greater than this, again indicating that sea-spray is not an important INP type in these CAO events.

On three flights (Table 2) two below-cloud filter samples were made at different points in the CAO. We might expect aerosol and INP scavenging to increase further south as CAOs develop, especially in the cumulus regime where intense precipitation might efficiently remove particles. A downwind decrease in aerosol number concentration in Norwegian Sea CAOs attributed to precipitation scavenging has previously been observed by Williams et al. (2024). Using the values of $N_{\text{INP}}(-15^{\circ}\text{C})$ and the total aerosol surface area S_{aer} , the factors of change in INP concentration (F_{INP}), ice-nucleating activity (F_{S}) and surface

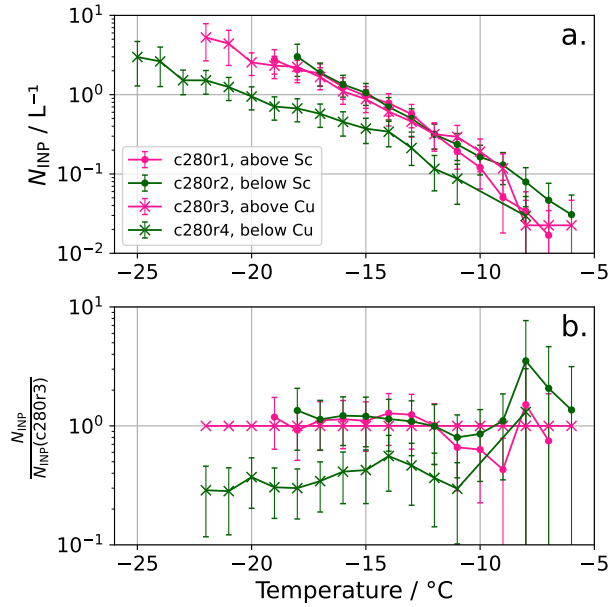


Figure 10. Panel a shows the four filter samples taken during flight c280 and describes their location relative to either stratocumulus (Sc) or cumulus (Cu) cloud. Panel b shows their INP concentrations relative to c280r3 (the sample taken above cumulus) for the temperature ranges which they can be compared.

area (F_{aer}) between the upstream and downstream measurements, upwind and downwind measurements,

$$F_{\text{INP}} = \frac{N_{\text{INP}}(-15^\circ\text{C, downstream})}{N_{\text{INP}}(-15^\circ\text{C, upstream})} \frac{N_{\text{INP}}(-15^\circ\text{C, downwind})}{N_{\text{INP}}(-15^\circ\text{C, upwind})}, \quad F_{\text{S}} = \frac{N_{\text{INP}}(-15^\circ\text{C, downstream})/S_{\text{aer}}}{N_{\text{INP}}(-15^\circ\text{C, upstream})/S_{\text{aer}}} \frac{N_{\text{INP}}(-15^\circ\text{C, downwind})}{N_{\text{INP}}(-15^\circ\text{C, upwind})} \quad (5)$$

were calculated. These values are displayed in Table 2 with the difference in latitude between the measurements, $\Delta\varphi$. Both the INP concentration and the ice-nucleating activity decreased with latitude. The total surface area of the aerosol increased in two flights by 70 and 90% and 69 and 85%, but decreased slightly by 25% in one pair. The upwind filters were sampled under stratocumulus conditions, while the downwind filters were in a mixture of stratocumulus and cumulus, with precipitation in two cases (c280r4 and c282r3). These c280r4 and c282r3.

460 During flight c280, two pairs of above and below-cloud filter samples were taken along the same wind trajectory (Figure 1b). The northern pair were taken where the clouds had stratocumulus forms, whereas the southern pair were taken where the clouds were in the cumulus regime. Comparing the INP spectra for these samples in Figure 10 shows that except at the very highest temperatures, where the error is large, there is little difference between the samples taken above and below the stratocumulus (c280r1 and c280r2, respectively) and the sample taken above the cumulus (c280r3). Closeness between the

three INP measurements may be expected if the main INP source entering the system is upwind of the CAO clouds. However, the southern sample taken below cumulus (c280r4) has over five times fewer INPs at temperatures below -11°C .

465 Together, these results are consistent with INP being removed by cloud and precipitation scavenging in the CAO, although this conclusion is based on only three cases. ~~In the future~~If precipitation scavenging is strong, it is possible that the INP concentrations measured during ACAO could be consistent with the INP concentrations measured at Andenes by Geerts et al. (2022). As such, it would be helpful to ~~have test this with future~~ aircraft INP measurements much deeper into the cumulus regime (i.e. further south)~~to test if the very low INP concentration reported by Geerts et al. (2022) are a result of precipitation scavenging.~~ This was not feasible in ACAO due to a combination of unfavourable meteorology, airspace restrictions and the prioritisation of tasks within the available flight time.

3.6 Backward trajectory analysis

To investigate the potential sources of sampled aerosol, backward trajectories were produced for each sample using the Hybrid Single-Particle Lagrangian Integrated Trajectory model (HYSPLIT) (Stein et al., 2015). Meteorological data from the Global
475 Data Assimilation System (GDAS) at 1° resolution was used to obtain the trajectories. The backward trajectories were run for seven days and initiated along each flight track at three-minute intervals during each of the sampling periods to produce multiple trajectories. Figure 11a shows these trajectories and Figure 11b shows the INP concentration at $T = -15^{\circ}\text{C}$ associated with each airmass. The majority of the airmasses associated with northerly cold-air outbreaks circulated in the high Arctic for several days. ~~Some of these passed over Asiatic mid-latitudes 6–7 days prior to sampling. In contrast, airmasses~~ Airmasses
480 ~~associated with westerly cold-air outbreaks (c273, c274)~~ CAOs (c273, c274) typically passed over Greenland, the Atlantic Ocean or Canada. ~~There~~ Some of the airmasses associated with northerly CAOs passed over Asiatic mid-latitudes 6–7 days prior to sampling. However, there was no clear correlation between INP concentration and airmass origin. ~~This is consistent with there being no distinct sources,~~ suggesting that the airmasses did not interact with a distinct source of INP in 7 days
485 transport. This might be consistent with a diffuse INP source across the whole of the Arctic region, or that the INP were emitted further back in time than 7 days ago and transported into the Arctic where they circulated around in the Arctic's stable atmosphere prior to being drawn out in CAO events. We return to these ideas in the next section.

4 Discussion of potential INP sources

The INP concentrations measured during the ACAO campaign were amongst some of the highest measured in the Arctic (Figure 3 and associated discussion). We now discuss several possible explanations for these high concentrations and thus the
490 potential sources of INPs.

If the INP were of local origin, strong local sources of INPs would be required to explain the high INP concentrations. Potential local sources of INPs in the region of the Norwegian Sea (Figure 1a) include upstream INP sources from Arctic land such as the Svalbard archipelago, continental INPs from Europe, sea-spray aerosol from the open sea, polynyas and open leads. However, there are several reasons why these Arctic sources are unlikely to play a major role.

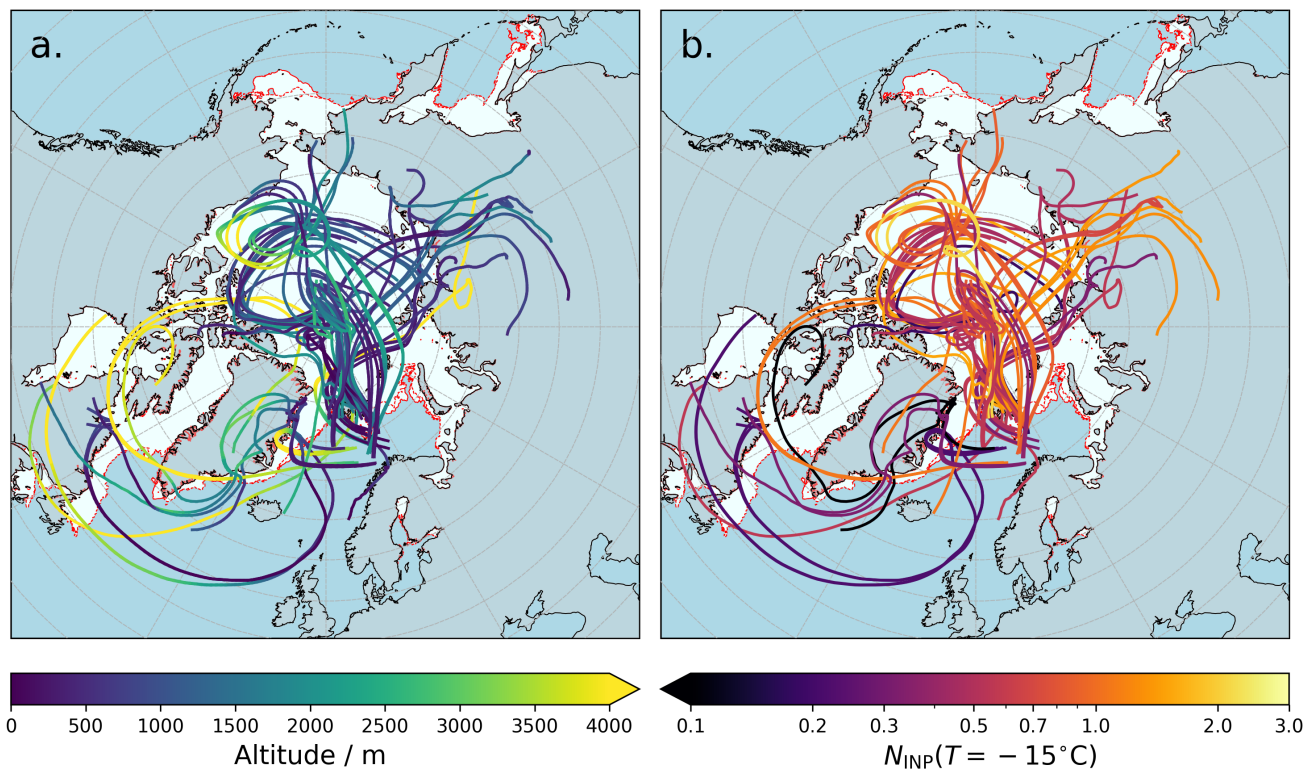


Figure 11. Seven-day backward trajectories of air masses sampled. Two trajectories are shown for each sample, corresponding to the start and end of the sampling periods. There was little variation in trajectories at intervals within the sampling periods. Panel **a** shows the altitudes associated with the trajectories, while panel **b** shows the relative magnitude of INP concentration, N_{INP} . Backward trajectories from [e272r6](#), measured in a warm-air intrusion, are not included.

495 The presence of dust indicated by the SEM analysis and the consistency of the measured active site densities shown in
 Figure 8 with those previously measured for biologically-enhanced mineral dusts could indicate a local terrestrial source
 of INPs. It has been shown that mineral dusts from high latitude sources contain ice-active biogenic materials (Barr et al.,
 2023; Tobo et al., 2019; Xi et al., 2022), hence dust might be sourced from the Svalbard archipelago or Greenland. However,
 back-trajectory analysis does not indicate that air masses directly from Svalbard or Greenland are consistently associated with
 500 the most active INP samples. Additionally, the pristine snow-cover over land in March means that emissions of aerosol are
 strongly suppressed and are therefore unlikely to dominate the INP population observed during ACAO (Bullard et al., 2016;
 Meinander et al., 2022). Although there have been reports of dust emission events on Svalbard happening as early in the year
 as May (Dörnbrack et al., 2010), these events in Svalbard are typically reported in autumn when snow cover is at its minimum
 (Meinander et al., 2022; Rymer et al., 2022).

505 It is also unlikely that transport of mid-latitude continental INPs from Europe directly into the cold-air outbreak regimes was a dominant source of INPs since the cold-air outbreak conditions exhibited northerly or westerly flows. Early in the campaign, there were prolonged warm-air intrusion conditions exhibiting south-westerly winds. However, some of the INP concentrations measured in the cold-air outbreak immediately after the warm-air intrusion had subsided (~~e273r2~~c273r2) were the lowest measured in the campaign.

510 Several aspects of the measurements suggest that sea-spray aerosol from the open sea was neither the dominant INP source nor a significant contributor to the ice-nucleating activity. Neither of the aerosol samples analysed with SEM showed that aerosols with clear sea-spray origins dominated the aerosol number, with less than 20% of the aerosol in the sample taken at an altitude of 155 m over the marginal ice zone having a sea-spray origin. In the boundary layer, the measured INP concentrations were several orders of magnitude higher than those measured in similarly remote areas in the Southern Ocean or the North
515 Atlantic where sea-spray aerosol is the dominant INP source (McCluskey et al., 2018a, b; Schmale et al., 2019; McFarquhar et al., 2021; Tatzelt et al., 2022). Furthermore, while the INP concentrations were similar above and below the cloud decks, the samples with highest active site density were found above the cloud systems and particularly upstream of the outbreak (Figure 9), environments unlikely to have large sea-spray components. Considering all these aspects, it is unlikely that sea-spray aerosol was a dominant source of INP.

520 ~~Another final~~ A final potential local source of INPs is the sea ice and leads in the sea ice. It has previously been hypothesised that open leads could be a significant source of INPs in the Arctic (Bigg and Leck, 2001). However, observed INP concentrations from ship campaigns passing through leads have found INP concentrations several orders of magnitude below those measured in ACAO (Bigg and Leck, 2001; Creamean et al., 2022). Furthermore, backward trajectories from the high Arctic measurements of INPs by Porter et al. (2022) showed that airmasses which had spent the majority of the past week over sea
525 ice had the lowest INP concentrations. Snow blown from the surface of sea ice has been shown to be a source of sea salt aerosol (~~Yang et al., 2008~~) (Yang et al., 2008; Gong et al., 2023), though there has been little investigation into this mechanism as a potential INP source, and the reduced activity of INP samples below the cloud deck again suggests that this would be unlikely to dominate the INP population. Together, these suggest that the sea ice was not a dominant source of INP during the ACAO campaign.

530 Further evidence against a local surface source of INP is that INP concentrations in northerly CAOs were fairly constant with altitude up to ~~3.5 km~~3 km (Fig 9). A local surface source would lead to enhanced INP at the surface in the highly stable stratified atmosphere of the Arctic in winter and early spring. However, high INP concentrations persistent during all flights between 21st and 30th March across a wide area. Additionally, there are no large-scale ascending air masses exiting the Arctic that would carry the aerosol to 3 km altitude, and convection is limited to altitudes lower than 2.5 km even in well-developed
535 CAOs.

Since it is unlikely that the dominant INPs had a local terrestrial or marine source, it follows that the high INP concentrations are likely to have originated by long-range transport. During the boreal winter aerosol in the Arctic atmosphere can then have lifetimes on the order of weeks or months as a result of the dry and stable conditions leading to weak aerosol scavenging (Carslaw, 2022). Coupled to this, we know that transport into the Arctic over the winter months leads to the build up of

540 pollution, dominantly from Eurasian sources that gives rise to the phenomenon of Arctic haze (Shaw, 1995; Stohl, 2006; Ekman and Schmale, 2022). While the anthropogenic component of Arctic haze has received substantial attention, it is also ~~well-know~~ than well-known that other mid- and low-latitude aerosol are transported into the Arctic along with this pollution aerosol, such as mineral dust from the African and Asian deserts (Rahn et al., 1977; Shi et al., 2022). Barrie (1986) suggested that the Arctic front extends as far south as 40° N in winter over the Eurasian land mass, encompassing sources such as the 545 Asian deserts as well as numerous pollution sources. Arctic haze layers have been reported to occur up to approximately 9 km altitude and have spacial extents on the order of 1000 km (Barrie, 1986). Our measurements of a widespread and vertically uniform distribution of INPs exiting the Arctic during the second half of March 2022 are consistent with a vertically extensive “reservoir” of INPs in the Arctic similar to pollution-related haze.

Previous airborne measurements of Arctic haze by Borys (1989) suggested that Arctic haze, when identified by large sig- 550 natures of anthropogenic pollutants, had 10–100 times fewer active INPs at -25°C than Arctic aerosol samples with fewer pollutants. However, these low-pollutant samples may have been transported into the Arctic from low-latitude INP-rich environments, like desert regions, without being mixed with anthropogenic sources. Accordingly, aerosol traditionally defined as Arctic haze due to its large pollution signature may not be associated with aerosol of lower latitude origin that has a high INP content. Springtime measurements of dust over the Norwegian Sea by Young et al. (2016) during the ACCACIA field cam- 555 paign were attributed to long-range transport and had elemental composition ratios similar to those from Asian dust. During the ACCACIA campaign, plumes of aerosol from eastern and northern Asia were observed, which were hypothesised to have transported dust to the region (Liu et al., 2015; Young et al., 2016). As mentioned above, Asian dust has been thought to be a source of Arctic Haze since the 1970s (Rahn et al., 1977), while recent modelling by Shi et al. (2022) showed that during the spring months, less than 20% of the Arctic dust load above 900 hPa was emitted in the Arctic and that approximately 50% of 560 the dust load at all heights came from Asia. Modelling by Groot Zwaaftink et al. (2016) also attributed approximately 38% of the Arctic dust load to Asian sources. This is significant since Asian dust is known to contain ice-active biological components (Creamean et al., 2013; Chen et al., 2021), which might be consistent with high ice-nucleating activities akin to those observed in ACAO. Transport routes for such biogenic containing Asian dust have been demonstrated by Zhao et al. (2022), while year- 565 round LIDAR observations by Ansmann et al. (2023) in the high Arctic have suggested that a small fraction of dust aerosols may control ice nucleation outside of the summer. Based on the above evidence, we suggest that the dominant INP observed in ACAO was mineral dust internally mixed with ice nucleating biogenic materials that originated from the lower latitudes and was transported into the Arctic through similar transport routes as Arctic haze.

The hypothesis of an INP reservoir appears to contradict previous remote sensing studies that use observations of Arctic clouds to infer spatial variations in INP concentrations. For instance, Carlsen and David (2022) define a temperature, T^* , at 570 which mixed-phase clouds become more frequent than liquid clouds, and use this as a proxy for freezing initiated by INP. They find that in winter, when Arctic haze builds up, T^* is lower over the sea-ice than the open sea, which they attributed to a suppression of INP emissions (and concentrations) caused by sea-ice cover. However, differences in ice concentrations between ice-covered and ice-free regions in high Arctic clouds may not reflect differences in INP concentration but rather differences in cloud microphysics related to cloud dynamics. For example, clouds over ice are shallow, long-lived and relatively

575 stable compared to the deeper clouds with colder tops over ocean regions (Morrison et al., 2012; Arteaga et al., 2024). The long
lifetime of these arctic clouds provides time for INP to be scavenged from the atmosphere, thus their small ice content may be a
consequence of their history rather than the INP concentration when they first formed. Similarly, Murray-Watson and Gryspeerd (2024)
used satellite observations to suggest that increasing ice concentrations downwind in CAOs imply increased INP concentrations
downwind, associating this with increased emissions of sea-spray INP. This contrasts with our linked in-situ measurements of
580 below-cloud INP that reveal a decrease in INP concentration downwind (Table 2). The increased downwind ice concentrations
observed by Murray-Watson and Gryspeerd (2024) may be related to secondary ice processes, rather than INP, since these are
associated with strongly-convective clouds which are more likely to occur downwind. Additionally, clouds later in the CAOs
tend to have lower cloud-top temperatures, naturally increasing the concentrations of ice.

5 Summary and conclusions

585 We ~~have~~ made the first airborne measurements of INPs targeted at cold-air outbreaks over the Norwegian and Barents seas.
We ~~made~~ took 23 filter measurements and performed droplet freezing assays using a droplet-on-filter technique to determine
INP concentration. INP concentrations measured over a large area of the Norwegian and Barents Seas ~~between 39 and 3403~~
~~m altitude at altitudes between 40–3400~~ m were amongst the highest reported in the Arctic, with $N_{\text{INP}}(-15^{\circ}\text{C})$ ranging
from ~~0.2–30.18–2.1~~ L^{-1} when the airflow had a strong northerly component. This indicates that high INP concentrations were
590 horizontally and vertically widespread in these northerly flows conducive to CAOs and boundary layer cloud formation, and
persisted for at least 12 days in late March. These high INP concentrations contrasted with previous surface measurements
made in the same region and at the same time of year, but overlap with other airborne measurements using an online measure-
ment technique. The lowest INP concentrations we measured during ACAO, ~~$N_{\text{INP}}(-15^{\circ}\text{C}) = 0.03$~~ $N_{\text{INP}}(-15^{\circ}\text{C}) = 0.03$ L^{-1} ,
were in a westerly CAO. These results, combined with the literature data highlight the importance of targeting INP measure-
595 ~~ments on~~ during specific meteorological events since an average INP concentration for this region and time would probably
not well-represent the INP population for specific CAO clouds.

To investigate the source of the high INP concentrations, we used particle-size data from the underwing probes of the aircraft
to normalise the INP concentration by the total aerosol surface area to gain an estimate of the density of active ice nucleation
sites across the samples. Comparing this to literature measurements of active site density suggested that the INP population
600 was likely ~~to be~~ dominated by mineral dust with ice-active biogenic components. Additionally, the samples with highest ice
active site densities were found above the cloud system, suggesting that the INP population was not dominated by sea-spray
aerosol. Scanning electron microscopy with energy-dispersive X-ray spectroscopy on two filters collected upstream in the
cold-air outbreaks showed the presence of mineral dusts accounting for 30% or more of the aerosol surface area. Considering
the meteorology during the campaign and activity of the samples, it is likely that the majority of the INPs did not come
605 from local sources, but instead came from long-range transport mechanisms more commonly associated with the Arctic Haze
phenomenon. As such, we suggest that the high INP concentrations measured during the ACAO campaign were due to the

presence of biogenically-enhanced dust, which dominated the ice nucleation processes rather than sea-spray aerosol in spite of the remoteness of the region.

610 These new measurements of INP concentrations measured in the ACAO campaign ~~raises~~raise important questions for our understanding of Arctic mixed-phase clouds. The strength of the cloud-phase feedback depends on the balance between ice and liquid in clouds in the present day, with clouds with more ice having a greater negative feedback on climate in a warming world (Murray et al., 2021). Our results suggest that the magnitude of the cloud-phase feedback may be larger in Northern Hemisphere CAOs compared to their Southern Ocean equivalents where it has been shown that the INP populations are many orders of magnitude smaller than in ACAO. Clearly, further work is needed to establish how representative ACAO was for
615 CAO conditions in the Arctic. Nevertheless, future modelling work should investigate the response of Arctic mixed-phase clouds with these INP concentrations to warming to reduce the uncertainty on this feedback.

The high INP concentrations measured in ACAO may also impact the transition between stratocumulus and cumulus clouds in CAOs, which is partially controlled by precipitation (Abel et al., 2017). Since enhanced INP concentration can enhance ice growth and thus enhance precipitation, these high INP concentrations may act as a control on CAO development. Modelling
620 that investigates the strength of control that INP concentration exhibits on CAO development would be useful to understand the impact of INPs on CAO cloud cover and thus radiative forcing. Finally, airborne measurements above and below the cloud deck have helped to establish the dominant INPs in these case studies. We recommend that more aircraft measurements are made in ~~regions where measurements of INP concentration have previously been dominated by ground studies~~air of direct relevance to clouds in order to better understand the relationship between cold-air outbreak cloud properties and INPs.

625 **Appendix A: Individual INP spectra and associated aerosol-size distributions**

Figures A1 and A2 show individually-labelled INP spectra and aerosol-size distributions respectively, as in Figures 3 and 5 where they are grouped by location relative to cloud.

Appendix B: INP spectra curve fitting

630 Our measurements show that the entire INP spectrum ($N_{\text{INP}}(T)$) varied over the campaign (Figure 3). To represent the INP concentration across the full temperature spectrum in future modelling work, particularly when modelling individual case studies, we fitted all spectra to a four-parameter function. This function took the form

$$\underline{N_{\text{INP}} = \nu_{\text{INP}} \exp \left[a (T_{\text{max}} - T)^b \right]}, \quad (\text{B1})$$

The parameter T_{max} represents the greatest temperature at which a freezing event was observed, a and b are shape parameters that determine the curvature of the function, and ν_{INP} is a scale parameter related to INP concentrations (if the shape were
635 constant). For INP spectra with the same shape, greater values of ν_{INP} indicate greater INP concentrations across the entire

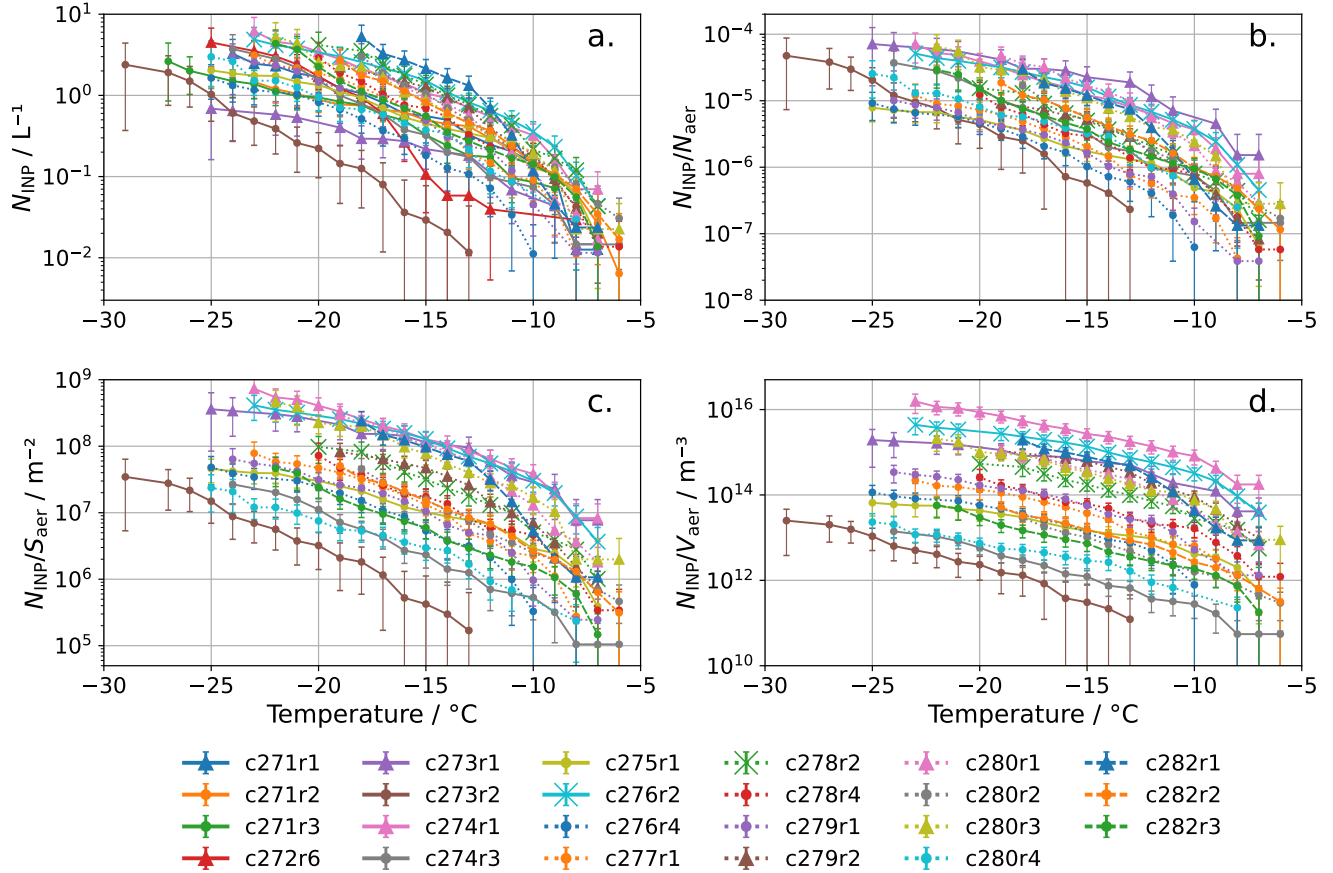


Figure A1. Parametrisations of Panel a shows INP concentration concentrations for each sample made during the campaign. Panels b, c and d show these concentrations normalised by the total number (N_{aer}), surface area according to Eqs. B1 (S_{aer}) and B2 respectively. There is no parametrisation volume (V_{aer}) of $N_{\text{INP}}/S_{\text{aer}}$ for flights c271 and c272 due to a lack of aerosol-size data. Similar parametrisations for INP concentration normalised by $N_{\text{aer}} V_{\text{aer}}$, not presented in this paper, can be found aerosols with other metadata at diameters greater than 0.1 μm .

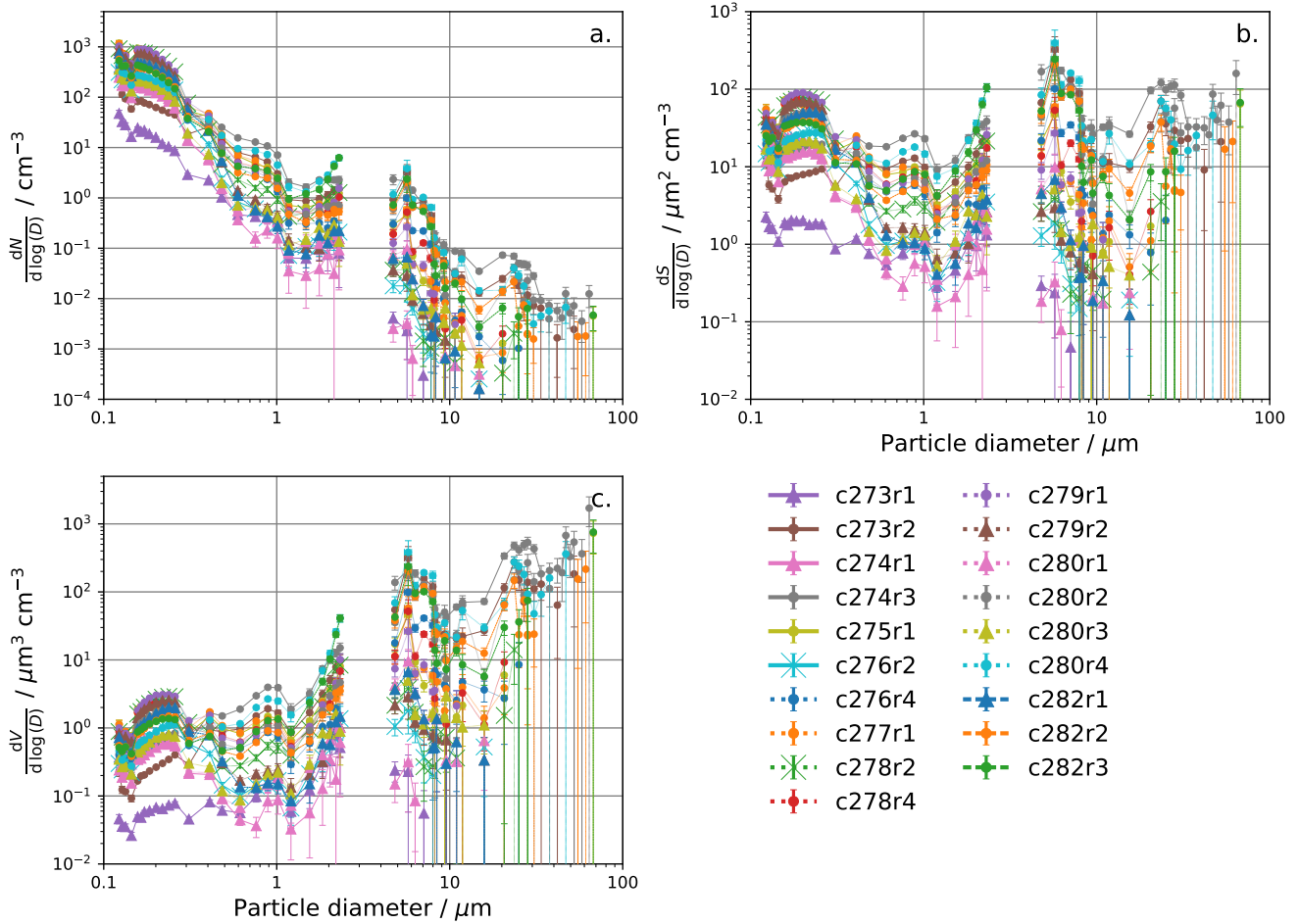


Figure A2. Size distributions of **a** particle number, **b** particle surface area and **c** particle volume measured with the PCASP and CDP probes during each filter sample. Probe data was unavailable during flights c271 and c272.

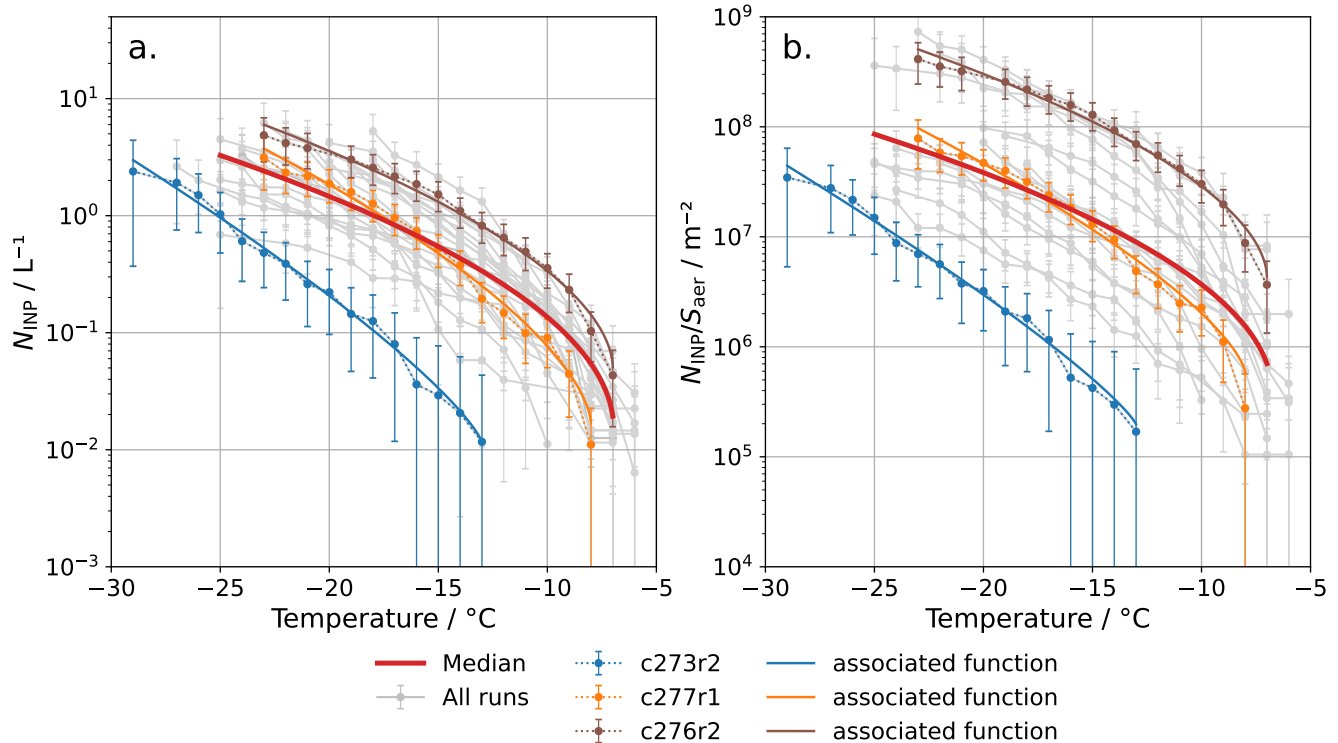


Figure B1. All measured temperature spectra for (a) INP concentration and (b) INP concentration normalised by aerosol surface area were fitted to Eq. B1 and B2 respectively. In both panels, examples of fits to randomly-chosen spectra with relatively high, medium and low INP spectra are demonstrated. In panel a, the red line shows the function fitted to the median INP concentration observed during the campaign, where $\nu_{\text{INP}} = 1.480 \times 10^{-2} \text{ L}^{-1}$, $T_{\text{max}} = 266.2 \text{ K}$, $a = 1.271 \text{ K}^{-b}$ and $b = 0.5$. In panel b, the red line shows the function fitted to the median active site density observed during the campaign, where $\nu_{\text{S}} = 3.712 \times 10^5 \text{ m}^{-2}$, $T_{\text{max}} = 266.4 \text{ K}$, $a = 1.273 \text{ K}^{-b}$ and $b = 0.5$.

temperature range. The same functional form was also applied to active site density spectra, which were fitted to the equation

$$N_{\text{INP}}/S_{\text{aer}} = \nu_{\text{S}} \exp \left[a (T_{\text{max}} - T)^b \right] \quad (\text{B2})$$

Fitting parameters for all spectra are given in Table B1, while examples of this fitting are shown in Figure B1, where functions for three individual samples, c273r2, c277r1 and c276r2 are illustrated. These represent filter measurements with low, medium and high INP concentrations and active site densities and demonstrate the ability of the function to represent all INP concentrations during the campaign. Equations B1 and B2 were also used to create parametrisations for the median INP concentration and active site density across the campaign for springtime CAOs in the region (excluding c272r6, which was not made in cold-air outbreak conditions). These are also shown in Figure B1.

Code and data availability. Code used for analysis and the creation of the figures in this notebook can be found at <https://doi.org/10.5281/zenodo.11221398>. Raw and processed INP data and metadata, processed aerosol-size data and INP data normalised by this (e.g. $N_{\text{INP}}/S_{\text{aer}}$), HYSPLIT inputs and outputs and Nevzorov clear-air flags are contained can be found at <https://doi.org/10.5281/zenodo.11221599>. Flight data from the FAAM aircraft are stored on the CEDA archive at <https://catalogue.ceda.ac.uk/uuid/01021a90c0c2481c909bdb145cb72398>.

Author contributions. The work was conceptualised by ENR, KSC, BJM, PRF, SJA and SLB. Flights were planned by SJA, PAB, KNB, PRF, BJM and ENR. Experiments were carried out by SLB, MDT, JBM, BJM, MID and ENR. Formal analysis was carried out by ENR while data was curated by ENR, MID and SJA. Python code was written by ENR and SLB. The original draft was written by ENR and was reviewed by all authors. The work was supervised by KSC, BJM and PRF. Funding was acquired by BJM.

Competing interests. KSC is an editor of Atmospheric Chemistry and Physics.

Acknowledgements. The samples were collected using the FAAM BAe-146-301 Atmospheric Research Aircraft, flown by Airtask Ltd., maintained by Avalon Aero Ltd. and managed by FAAM Airborne Laboratory. The FAAM Airborne Laboratory is jointly operated by UK Research and Innovation and the University of Leeds. We are grateful to all of the people from the Met Office, the University of Leeds, the University of Manchester, FAAM, Airtask and Avalon Aero that were instrumental in making the ACAO campaign a success. This work used JASMIN, the UK collaborative data analysis facility. We thank Alberto Sanchez-Marroquin (now at the Barcelona Supercomputing Center) for assistance with the scanning electron microscopy analysis. We acknowledge the use of imagery provided by services from NASA's Global Imagery Browse Services (GIBS), part of NASA's Earth Observing System Data and Information System (EOSDIS). We thank Armin Sorooshian and the anonymous reviewer for insightful comments that significantly improved this work. Additionally, we thank Cameron Belton for alerting us to typographical errors in the original manuscript.

We acknowledge the use of reanalysis data provided by the Copernicus Climate Change Service 2020. The ACAO flight campaign was largely funded by the Met Office, with a contribution of additional flight hours from M-Phase. M-Phase was supported by the Natural Environment Research Council (NERC) as part of the CloudSense Programme (M-Phase: NE/T00648X/1 and NE/T006463/1; and DCMEX: NE/T006420/1). ENR was supported by the NERC Panorama Doctoral Training programme of NERC, grant number Programme (NE/S007458/1). SLB was funded by an Industrial CASE studentship from NERC (NE/R006687/1).

References

- Abel, S. J., Cotton, R. J., Barrett, P. A., and Vance, A. K.: A comparison of ice water content measurement techniques on the FAAM BAe-146 aircraft, *Atmospheric Measurement Techniques*, 7, 3007–3022, <https://doi.org/10.5194/amt-7-3007-2014>, publisher: Copernicus GmbH, 2014.
- Abel, S. J., Boutle, I. A., Waite, K., Fox, S., Brown, P. R. A., Cotton, R., Lloyd, G., Choulaton, T. W., and Bower, K. N.: The Role of Precipitation in Controlling the Transition from Stratocumulus to Cumulus Clouds in a Northern Hemisphere Cold-Air Outbreak, *Journal of the Atmospheric Sciences*, 74, 2293–2314, <https://doi.org/10.1175/JAS-D-16-0362.1>, publisher: American Meteorological Society Section: Journal of the Atmospheric Sciences, 2017.
- Andreae, M. O., Berresheim, H., Andreae, T. W., Kritz, M. A., Bates, T. S., and Merrill, J. T.: Vertical distribution of dimethylsulfide, sulfur dioxide, aerosol ions, and radon over the Northeast Pacific Ocean, *Journal of Atmospheric Chemistry*, 6, 149–173, <https://doi.org/10.1007/BF00048337>, 1988.
- Andreae, M. O., Elbert, W., Gabriel, R., Johnson, D. W., Osborne, S., and Wood, R.: Soluble ion chemistry of the atmospheric aerosol and SO₂ concentrations over the eastern North Atlantic during ACE-2, *Tellus B: Chemical and Physical Meteorology*, 52, 1066–1087, <https://doi.org/10.3402/tellusb.v52i4.17087>, publisher: Taylor & Francis _eprint: <https://doi.org/10.3402/tellusb.v52i4.17087>, 2000.
- Ansmann, A., Ohneiser, K., Engelmann, R., Radenz, M., Griesche, H., Hofer, J., Althausen, D., Creamean, J. M., Boyer, M. C., Knopf, D. A., Dahlke, S., Maturilli, M., Gebauer, H., Bühl, J., Jimenez, C., Seifert, P., and Wandinger, U.: Annual cycle of aerosol properties over the central Arctic during MOSAiC 2019–2020 – light-extinction, CCN, and INP levels from the boundary layer to the tropopause, *Atmospheric Chemistry and Physics*, 23, 12 821–12 849, <https://doi.org/10.5194/acp-23-12821-2023>, publisher: Copernicus GmbH, 2023.
- Arteaga, D., Planche, C., Tridon, F., Dupuy, R., Baudoux, A., Banson, S., Baray, J.-L., Mioche, G., Ehrlich, A., Mech, M., Mertes, S., Wendisch, M., Wobrock, W., and Jourdan, O.: Arctic mixed-phase clouds simulated by the WRF model: Comparisons with ALOUD radar and *in situ* airborne observations and sensitivity of microphysics properties, *Atmospheric Research*, 307, 107 471, <https://doi.org/10.1016/j.atmosres.2024.107471>, 2024.
- Barr, S. L.: The sources and activity of ice-nucleating particles in the high latitudes, phd, University of Leeds, <https://etheses.whiterose.ac.uk/33752/>, 2023.
- Barr, S. L., Wyld, B., McQuaid, J. B., Neely III, R. R., and Murray, B. J.: Southern Alaska as a source of atmospheric mineral dust and ice-nucleating particles, *Science Advances*, 9, eadg3708, <https://doi.org/10.1126/sciadv.adg3708>, publisher: American Association for the Advancement of Science, 2023.
- Barrett, P. A., Blyth, A., Brown, P. R. A., and Abel, S. J.: The structure of turbulence and mixed-phase cloud microphysics in a highly supercooled altocumulus cloud, *Atmospheric Chemistry and Physics*, 20, 1921–1939, <https://doi.org/10.5194/acp-20-1921-2020>, publisher: Copernicus GmbH, 2020.
- Barrie, L. A.: Arctic air pollution: An overview of current knowledge, *Atmospheric Environment* (1967), 20, 643–663, [https://doi.org/10.1016/0004-6981\(86\)90180-0](https://doi.org/10.1016/0004-6981(86)90180-0), 1986.
- Beall, C. M., Lucero, D., Hill, T. C., DeMott, P. J., Stokes, M. D., and Prather, K. A.: Best practices for precipitation sample storage for offline studies of ice nucleation in marine and coastal environments, *Atmospheric Measurement Techniques*, 13, 6473–6486, <https://doi.org/10.5194/amt-13-6473-2020>, publisher: Copernicus GmbH, 2020.

- Bergeron, T.: On the Physics of Cloud and Precipitation, *Nippon Sugaku-Buturigakkwaishi*, 9, 446–448, <https://doi.org/10.11429/subutsukaishi1927.9.446>, publisher: THE PHYSICAL SOCIETY OF JAPAN , The Mathematical Society of Japan, 1935.
- 705 Bigg, E. K. and Leck, C.: Cloud-active particles over the central Arctic Ocean, *Journal of Geophysical Research: Atmospheres*, 106, 32 155–32 166, <https://doi.org/10.1029/1999JD901152>, _eprint: <https://onlinelibrary.wiley.com/doi/pdf/10.1029/1999JD901152>, 2001.
- Borys, R. D.: Studies of ice nucleation by Arctic aerosol on AGASP-II, *Journal of Atmospheric Chemistry*, 9, 169–185, <https://doi.org/10.1007/BF00052831>, 1989.
- Brasseur, Z., Castarède, D., Thomson, E. S., Adams, M. P., Drossaert van Dusseldorp, S., Heikkilä, P., Korhonen, K., Lampilahti, J., Paramonov, M., Schneider, J., Vogel, F., Wu, Y., Abbatt, J. P. D., Atanasova, N. S., Bamford, D. H., Bertozzi, B., Boyer, M., Brus, D., Daily, M. I., Fösig, R., Gute, E., Harrison, A. D., Hietala, P., Höhler, K., Kanji, Z. A., Keskinen, J., Lacher, L., Lampimäki, M., Levula, J., Manninen, A., Nadolny, J., Peltola, M., Porter, G. C. E., Poutanen, P., Proske, U., Schorr, T., Silas Umo, N., Stenszky, J., Virtanen, A., Moisseev, D., Kulmala, M., Murray, B. J., Petäjä, T., Möhler, O., and Duplissy, J.: Measurement report: Introduction to the HyICE-2018 campaign for measurements of ice-nucleating particles and instrument inter-comparison in the Hyttiälä boreal forest, *Atmospheric Chemistry and Physics*, 22, 5117–5145, <https://doi.org/10.5194/acp-22-5117-2022>, publisher: Copernicus GmbH, 2022.
- 710 Brümmer, B.: Boundary-layer modification in wintertime cold-air outbreaks from the Arctic sea ice, *Boundary-Layer Meteorology*, 80, 109–125, <https://doi.org/10.1007/BF00119014>, 1996.
- Bullard, J. E., Baddock, M., Bradwell, T., Crusius, J., Darlington, E., Gaiero, D., Gassó, S., Gisladottir, G., Hodgkins, R., McCulloch, R., McKenna-Neuman, C., Mockford, T., Stewart, H., and Thorsteinsson, T.: High-latitude dust in the Earth system, *Reviews of Geophysics*, 720 54, 447–485, <https://doi.org/10.1002/2016RG000518>, _eprint: <https://onlinelibrary.wiley.com/doi/pdf/10.1002/2016RG000518>, 2016.
- C3S: ERA5 hourly data on single levels from 1940 to present, <https://doi.org/10.24381/CDS.ADBB2D47>, 2018.
- Carlsen, T. and David, R. O.: Spaceborne Evidence That Ice-Nucleating Particles Influence High-Latitude Cloud Phase, *Geophysical Research Letters*, 49, e2022GL098 041, <https://doi.org/10.1029/2022GL098041>, _eprint: <https://onlinelibrary.wiley.com/doi/pdf/10.1029/2022GL098041>, 2022.
- 725 Carslaw, K. S.: Chapter 5 - Aerosol processes, in: *Aerosols and Climate*, edited by Carslaw, K. S., pp. 135–185, Elsevier, <https://doi.org/10.1016/B978-0-12-819766-0.00007-9>, 2022.
- Chen, J., Wu, Z., Chen, J., Reicher, N., Fang, X., Rudich, Y., and Hu, M.: Size-resolved atmospheric ice-nucleating particles during East Asian dust events, *Atmospheric Chemistry and Physics*, 21, 3491–3506, <https://doi.org/10.5194/acp-21-3491-2021>, publisher: Copernicus GmbH, 2021.
- 730 Creamean, J. M., Suski, K. J., Rosenfeld, D., Cazorla, A., DeMott, P. J., Sullivan, R. C., White, A. B., Ralph, F. M., Minnis, P., Comstock, J. M., Tomlinson, J. M., and Prather, K. A.: Dust and Biological Aerosols from the Sahara and Asia Influence Precipitation in the Western U.S., *Science*, 339, 1572–1578, <https://doi.org/10.1126/science.1227279>, publisher: American Association for the Advancement of Science, 2013.
- Creamean, J. M., Hill, T. C. J., DeMott, P. J., Uetake, J., Kreidenweis, S., and Douglas, T. A.: Thawing permafrost: an overlooked source of seeds for Arctic cloud formation, *Environmental Research Letters*, 15, 084 022, <https://doi.org/10.1088/1748-9326/ab87d3>, publisher: IOP Publishing, 2020.
- 735 Creamean, J. M., Barry, K., Hill, T. C. J., Hume, C., DeMott, P. J., Shupe, M. D., Dahlke, S., Willmes, S., Schmale, J., Beck, I., Hoppe, C. J. M., Fong, A., Chamberlain, E., Bowman, J., Scharien, R., and Persson, O.: Annual cycle observations of aerosols capable of ice

- formation in central Arctic clouds, *Nature Communications*, 13, 3537, <https://doi.org/10.1038/s41467-022-31182-x>, number: 1 Publisher: Nature Publishing Group, 2022.
- 740 DeMott, P. J., Hill, T. C. J., McCluskey, C. S., Prather, K. A., Collins, D. B., Sullivan, R. C., Ruppel, M. J., Mason, R. H., Irish, V. E., Lee, T., Hwang, C. Y., Rhee, T. S., Snider, J. R., McMeeking, G. R., Dhaniyala, S., Lewis, E. R., Wentzell, J. J. B., Abbatt, J., Lee, C., Sultana, C. M., Ault, A. P., Axson, J. L., Diaz Martinez, M., Venero, I., Santos-Figueroa, G., Stokes, M. D., Deane, G. B., Mayol-Bracero, O. L., Grassian, V. H., Bertram, T. H., Bertram, A. K., Moffett, B. F., and Franc, G. D.: Sea spray aerosol as a unique source of ice nucleating particles, *Proceedings of the National Academy of Sciences*, 113, 5797–5803, <https://doi.org/10.1073/pnas.1514034112>, publisher: Proceedings of the National Academy of Sciences, 2016.
- 745 DeMott, P. J., Möhler, O., Cziczo, D. J., Hiranuma, N., Petters, M. D., Petters, S. S., Belosi, F., Bingemer, H. G., Brooks, S. D., Budke, C., Burkert-Kohn, M., Collier, K. N., Danielczok, A., Eppers, O., Felgitsch, L., Garimella, S., Grothe, H., Herenz, P., Hill, T. C. J., Höhler, K., Kanji, Z. A., Kiselev, A., Koop, T., Kristensen, T. B., Krüger, K., Kulkarni, G., Levin, E. J. T., Murray, B. J., Nicosia, A., O’Sullivan, D., Peckhaus, A., Polen, M. J., Price, H. C., Reicher, N., Rothenberg, D. A., Rudich, Y., Santachiara, G., Schiebel, T., Schrod, J., Seifried, T. M., Stratmann, F., Sullivan, R. C., Suski, K. J., Szakáll, M., Taylor, H. P., Ullrich, R., Vergara-Temprado, J., Wagner, R., Whale, T. F., Weber, D., Welti, A., Wilson, T. W., Wolf, M. J., and Zenker, J.: The Fifth International Workshop on Ice Nucleation phase 2 (FIN-02): laboratory intercomparison of ice nucleation measurements, *Atmospheric Measurement Techniques*, 11, 6231–6257, <https://doi.org/10.5194/amt-11-6231-2018>, publisher: Copernicus GmbH, 2018.
- 750 Dörnbrack, A., Stachlewska, I. S., Ritter, C., and Neuber, R.: Aerosol distribution around Svalbard during intense easterly winds, *Atmospheric Chemistry and Physics*, 10, 1473–1490, <https://doi.org/10.5194/acp-10-1473-2010>, publisher: Copernicus GmbH, 2010.
- 755 Ekman, A. M. L. and Schmale, J.: Chapter 16 - Aerosol processes in high-latitude environments and the effects on climate, in: *Aerosols and Climate*, edited by Carslaw, K. S., pp. 651–706, Elsevier, <https://doi.org/10.1016/B978-0-12-819766-0.00005-5>, 2022.
- Field, P. R., Lawson, R. P., Brown, P. R. A., Lloyd, G., Westbrook, C., Moisseev, D., Miltenberger, A., Nenes, A., Blyth, A., Choulaton, T., Connolly, P., Buehl, J., Crosier, J., Cui, Z., Dearden, C., DeMott, P., Flossmann, A., Heymsfield, A., Huang, Y., Kalesse, H., Kanji, Z. A., Korolev, A., Kirchgaessner, A., Lasher-Trapp, S., Leisner, T., McFarquhar, G., Phillips, V., Stith, J., and Sullivan, S.: Secondary Ice Production: Current State of the Science and Recommendations for the Future, *Meteorological Monographs*, 58, 7.1–7.20, <https://doi.org/10.1175/AMSMONOGRAPHS-D-16-0014.1>, publisher: American Meteorological Society Section: Meteorological Monographs, 2017.
- 760 Findeisen, W.: Die kolloidmeteorologischen Vorgänge bei der Niederschlagsbildung, *Meteorological Zeitschrift*, 55, 121–133, 1938.
- 765 Fletcher, J., Mason, S., and Jakob, C.: The Climatology, Meteorology, and Boundary Layer Structure of Marine Cold Air Outbreaks in Both Hemispheres, *Journal of Climate*, 29, 1999–2014, <https://doi.org/10.1175/JCLI-D-15-0268.1>, publisher: American Meteorological Society Section: Journal of Climate, 2016a.
- Fletcher, J. K., Mason, S., and Jakob, C.: A Climatology of Clouds in Marine Cold Air Outbreaks in Both Hemispheres, *Journal of Climate*, 29, 6677–6692, <https://doi.org/10.1175/JCLI-D-15-0783.1>, publisher: American Meteorological Society Section: Journal of Climate, 2016b.
- 770 Garrett, T. J., Hobbs, P. V., and Gerber, H.: Shortwave, single-scattering properties of arctic ice clouds, *Journal of Geophysical Research: Atmospheres*, 106, 15 155–15 172, <https://doi.org/10.1029/2000JD900195>, _eprint: <https://onlinelibrary.wiley.com/doi/pdf/10.1029/2000JD900195>, 2001.
- 775 Geerts, B., Giangrande, S. E., McFarquhar, G. M., Xue, L., Abel, S. J., Comstock, J. M., Crewell, S., DeMott, P. J., Ebell, K., Field, P., Hill, T. C. J., Hunzinger, A., Jensen, M. P., Johnson, K. L., Juliano, T. W., Kollias, P., Kosovic, B., Lackner, C., Luke, E., Lüpkes, C., Matthews,

- A. A., Neggers, R., Ovchinnikov, M., Powers, H., Shupe, M. D., Spengler, T., Swanson, B. E., Tjernström, M., Theisen, A. K., Wales, N. A., Wang, Y., Wendisch, M., and Wu, P.: The COMBLE Campaign: A Study of Marine Boundary Layer Clouds in Arctic Cold-Air Outbreaks, *Bulletin of the American Meteorological Society*, 103, E1371–E1389, <https://doi.org/10.1175/BAMS-D-21-0044.1>, publisher: American Meteorological Society Section: Bulletin of the American Meteorological Society, 2022.
- 780 Gjelsvik, A. B., David, R. O., Carlsen, T., Hellmuth, F., Hofer, S., McGraw, Z., Sodemann, H., and Storelvmo, T.: Using a region-specific ice-nucleating particle parameterization improves the representation of Arctic clouds in a global climate model, *EGUsphere*, pp. 1–32, <https://doi.org/10.5194/egusphere-2024-1879>, publisher: Copernicus GmbH, 2024.
- Gong, X., Zhang, J., Croft, B., Yang, X., Frey, M. M., Bergner, N., Chang, R. Y.-W., Creamean, J. M., Kuang, C., Martin, R. V., Ranjithkumar, A., Sedlacek, A. J., Uin, J., Willmes, S., Zawadowicz, M. A., Pierce, J. R., Shupe, M. D., Schmale, J., and Wang, J.: Arctic warming by abundant fine sea salt aerosols from blowing snow, *Nature Geoscience*, 16, 768–774, <https://doi.org/10.1038/s41561-023-01254-8>, publisher: Nature Publishing Group, 2023.
- 785 Groot Zwaafink, C. D., Grythe, H., Skov, H., and Stohl, A.: Substantial contribution of northern high-latitude sources to mineral dust in the Arctic, *Journal of Geophysical Research: Atmospheres*, 121, 13,678–13,697, <https://doi.org/10.1002/2016JD025482>, [_eprint: https://onlinelibrary.wiley.com/doi/pdf/10.1002/2016JD025482](https://onlinelibrary.wiley.com/doi/pdf/10.1002/2016JD025482), 2016.
- 790 Hallett, J. and Mossop, S. C.: Production of secondary ice particles during the riming process, *Nature*, 249, 26–28, <https://doi.org/10.1038/249026a0>, bandiera_abtest: a Cg_type: Nature Research Journals Number: 5452 Primary_atype: Research Publisher: Nature Publishing Group, 1974.
- Harrison, A. D., Lever, K., Sanchez-Marroquin, A., Holden, M. A., Whale, T. F., Tarn, M. D., McQuaid, J. B., and Murray, B. J.: The ice-nucleating ability of quartz immersed in water and its atmospheric importance compared to K-feldspar, *Atmospheric Chemistry and Physics*, 19, 11 343–11 361, <https://doi.org/10.5194/acp-19-11343-2019>, publisher: Copernicus GmbH, 2019.
- 795 Hartmann, M., Adachi, K., Eppers, O., Haas, C., Herber, A., Holzinger, R., Hünerbein, A., Jäkel, E., Jentsch, C., van Pinxteren, M., Wex, H., Willmes, S., and Stratmann, F.: Wintertime Airborne Measurements of Ice Nucleating Particles in the High Arctic: A Hint to a Marine, Biogenic Source for Ice Nucleating Particles, *Geophysical Research Letters*, 47, e2020GL087 770, <https://doi.org/10.1029/2020GL087770>, [_eprint: https://onlinelibrary.wiley.com/doi/pdf/10.1029/2020GL087770](https://onlinelibrary.wiley.com/doi/pdf/10.1029/2020GL087770), 2020.
- 800 Hartmann, M., Gong, X., Kecorius, S., van Pinxteren, M., Vogl, T., Welti, A., Wex, H., Zeppenfeld, S., Herrmann, H., Wiedensohler, A., and Stratmann, F.: Terrestrial or marine – indications towards the origin of ice-nucleating particles during melt season in the European Arctic up to 83.7°N, *Atmospheric Chemistry and Physics*, 21, 11 613–11 636, <https://doi.org/10.5194/acp-21-11613-2021>, publisher: Copernicus GmbH, 2021.
- 805 Herbert, R. J., Murray, B. J., Dobbie, S. J., and Koop, T.: Sensitivity of liquid clouds to homogenous freezing parameterizations, *Geophysical Research Letters*, 42, 1599–1605, <https://doi.org/10.1002/2014GL062729>, [_eprint: https://onlinelibrary.wiley.com/doi/pdf/10.1002/2014GL062729](https://onlinelibrary.wiley.com/doi/pdf/10.1002/2014GL062729), 2015.
- Hiranuma, N., Adachi, K., Bell, D. M., Belosi, F., Beydoun, H., Bhaduri, B., Bingemer, H., Budke, C., Clemen, H.-C., Conen, F., Cory, K. M., Curtius, J., DeMott, P. J., Eppers, O., Grawe, S., Hartmann, S., Hoffmann, N., Höhler, K., Jantsch, E., Kiselev, A., Koop, T., Kulkarni, G., Mayer, A., Murakami, M., Murray, B. J., Nicosia, A., Petters, M. D., Piazza, M., Polen, M., Reicher, N., Rudich, Y., Saito, A., Santachiara, G., Schiebel, T., Schill, G. P., Schneider, J., Segev, L., Stopelli, E., Sullivan, R. C., Suski, K., Szakáll, M., Tajiri, T., Taylor, H., Tobo, Y., Ullrich, R., Weber, D., Wex, H., Whale, T. F., Whiteside, C. L., Yamashita, K., Zelenyuk, A., and Möhler, O.: A comprehensive characterization of ice nucleation by three different types of cellulose particles immersed in water, *Atmospheric Chemistry and Physics*, 19, 4823–4849, <https://doi.org/10.5194/acp-19-4823-2019>, publisher: Copernicus GmbH, 2019.

- 815 Huang, S., Hu, W., Chen, J., Wu, Z., Zhang, D., and Fu, P.: Overview of biological ice nucleating particles in the atmosphere, *Environment International*, 146, 106 197, <https://doi.org/10.1016/j.envint.2020.106197>, 2021.
- Ickes, L., Welti, A., Hoose, C., and Lohmann, U.: Classical nucleation theory of homogeneous freezing of water: thermodynamic and kinetic parameters, *Physical Chemistry Chemical Physics*, 17, 5514–5537, <https://doi.org/10.1039/C4CP04184D>, publisher: The Royal Society of Chemistry, 2015.
- 820 Kanji, Z. A., Ladino, L. A., Wex, H., Boose, Y., Burkert-Kohn, M., Cziczo, D. J., and Krämer, M.: Overview of Ice Nucleating Particles, *Meteorological Monographs*, 58, 1.1–1.33, <https://doi.org/10.1175/AMSMONOGRAPHS-D-16-0006.1>, publisher: American Meteorological Society Section: Meteorological Monographs, 2017.
- Kawai, K., Matsui, H., and Tobo, Y.: Dominant Role of Arctic Dust With High Ice Nucleating Ability in the Arctic Lower Troposphere, *Geophysical Research Letters*, 50, e2022GL102 470, <https://doi.org/10.1029/2022GL102470>, [_eprint: https://onlinelibrary.wiley.com/doi/pdf/10.1029/2022GL102470](https://onlinelibrary.wiley.com/doi/pdf/10.1029/2022GL102470), 2023.
- 825 Knopf, D. A., Wang, P., Wong, B., Tomlin, J. M., Veghte, D. P., Lata, N. N., China, S., Laskin, A., Moffet, R. C., Aller, J. Y., Marcus, M. A., and Wang, J.: Physicochemical characterization of free troposphere and marine boundary layer ice-nucleating particles collected by aircraft in the eastern North Atlantic, *Atmospheric Chemistry and Physics*, 23, 8659–8681, <https://doi.org/10.5194/acp-23-8659-2023>, publisher: Copernicus GmbH, 2023.
- 830 Korolev, A. and Leisner, T.: Review of experimental studies of secondary ice production, *Atmospheric Chemistry and Physics*, 20, 11 767–11 797, <https://doi.org/10.5194/acp-20-11767-2020>, publisher: Copernicus GmbH, 2020.
- Korolev, A., McFarquhar, G., Field, P. R., Franklin, C., Lawson, P., Wang, Z., Williams, E., Abel, S. J., Axisa, D., Borrmann, S., Crosier, J., Fugal, J., Krämer, M., Lohmann, U., Schlenczek, O., Schnaiter, M., and Wendisch, M.: Mixed-Phase Clouds: Progress and Challenges, *Meteorological Monographs*, 58, 5.1–5.50, <https://doi.org/10.1175/AMSMONOGRAPHS-D-17-0001.1>, publisher: American Meteorological Society Section: Meteorological Monographs, 2017.
- 835 Korolev, A. V., Strapp, J. W., Isaac, G. A., and Nevzorov, A. N.: The Nevzorov Airborne Hot-Wire LWC–TWC Probe: Principle of Operation and Performance Characteristics, *Journal of Atmospheric and Oceanic Technology*, 15, 1495–1510, [https://doi.org/10.1175/1520-0426\(1998\)015<1495:TNAHWL>2.0.CO;2](https://doi.org/10.1175/1520-0426(1998)015<1495:TNAHWL>2.0.CO;2), publisher: American Meteorological Society Section: Journal of Atmospheric and Oceanic Technology, 1998.
- 840 Lacher, L., Adams, M. P., Barry, K., Bertozzi, B., Bingemer, H., Boffo, C., Bras, Y., Büttner, N., Castarede, D., Cziczo, D. J., DeMott, P. J., Fösig, R., Goodell, M., Höhler, K., Hill, T. C. J., Jentsch, C., Ladino, L. A., Levin, E. J. T., Mertes, S., Möhler, O., Moore, K. A., Murray, B. J., Nadolny, J., Pfeuffer, T., Picard, D., Ramírez-Romero, C., Ribeiro, M., Richter, S., Schrod, J., Sellegri, K., Stratmann, F., Swanson, B. E., Thomson, E. S., Wex, H., Wolf, M. J., and Freney, E.: The Puy de Dôme ICe Nucleation Intercomparison Campaign (PICNIC): comparison between online and offline methods in ambient air, *Atmospheric Chemistry and Physics*, 24, 2651–2678, <https://doi.org/10.5194/acp-24-2651-2024>, publisher: Copernicus GmbH, 2024.
- 845 Latimer, R. N. C. and Martin, R. V.: Interpretation of measured aerosol mass scattering efficiency over North America using a chemical transport model, *Atmospheric Chemistry and Physics*, 19, 2635–2653, <https://doi.org/10.5194/acp-19-2635-2019>, publisher: Copernicus GmbH, 2019.
- Li, G., Wilbourn, E. K., Cheng, Z., Wieder, J., Fagerson, A., Henneberger, J., Motos, G., Traversi, R., Brooks, S. D., Mazzola, M., China, S., Nenes, A., Lohmann, U., Hiranuma, N., and Kanji, Z. A.: Physicochemical characterization and source apportionment of Arctic ice-nucleating particles observed in Ny-Ålesund in autumn 2019, *Atmospheric Chemistry and Physics*, 23, 10 489–10 516, <https://doi.org/10.5194/acp-23-10489-2023>, publisher: Copernicus GmbH, 2023.

- Liu, D., Quennehen, B., Darbyshire, E., Allan, J. D., Williams, P. I., Taylor, J. W., Bauguitte, S. J.-B., Flynn, M. J., Lowe, D., Gallagher, M. W., Bower, K. N., Choularton, T. W., and Coe, H.: The importance of Asia as a source of black carbon to the European Arctic during springtime 2013, *Atmospheric Chemistry and Physics*, 15, 11 537–11 555, <https://doi.org/10.5194/acp-15-11537-2015>, publisher: Copernicus GmbH, 2015.
- Martin, R. V., Jacob, D. J., Yantosca, R. M., Chin, M., and Ginoux, P.: Global and regional decreases in tropospheric oxidants from photochemical effects of aerosols, *Journal of Geophysical Research: Atmospheres*, 108, <https://doi.org/10.1029/2002JD002622>, <https://onlinelibrary.wiley.com/doi/pdf/10.1029/2002JD002622>, 2003.
- 855 McCluskey, C. S., Hill, T. C. J., Humphries, R. S., Rauker, A. M., Moreau, S., Stratton, P. G., Chambers, S. D., Williams, A. G., McRobert, I., Ward, J., Keywood, M. D., Harnwell, J., Ponsonby, W., Loh, Z. M., Krummel, P. B., Protat, A., Kreidenweis, S. M., and DeMott, P. J.: Observations of Ice Nucleating Particles Over Southern Ocean Waters, *Geophysical Research Letters*, 45, 11,989–11,997, <https://doi.org/10.1029/2018GL079981>, [eprint: https://onlinelibrary.wiley.com/doi/pdf/10.1029/2018GL079981](https://onlinelibrary.wiley.com/doi/pdf/10.1029/2018GL079981), 2018a.
- 860 McCluskey, C. S., Ovadnevaite, J., Rinaldi, M., Atkinson, J., Belosi, F., Ceburnis, D., Marullo, S., Hill, T. C. J., Lohmann, U., Kanji, Z. A., O'Dowd, C., Kreidenweis, S. M., and DeMott, P. J.: Marine and Terrestrial Organic Ice-Nucleating Particles in Pristine Marine to Continentally Influenced Northeast Atlantic Air Masses, *Journal of Geophysical Research: Atmospheres*, 123, 6196–6212, <https://doi.org/10.1029/2017JD028033>, [eprint: https://onlinelibrary.wiley.com/doi/pdf/10.1029/2017JD028033](https://onlinelibrary.wiley.com/doi/pdf/10.1029/2017JD028033), 2018b.
- 870 McFarquhar, G. M., Bretherton, C. S., Marchand, R., Protat, A., DeMott, P. J., Alexander, S. P., Roberts, G. C., Twohy, C. H., Toohey, D., Siems, S., Huang, Y., Wood, R., Rauber, R. M., Lasher-Trapp, S., Jensen, J., Stith, J. L., Mace, J., Um, J., Järvinen, E., Schnaiter, M., Gettelman, A., Sanchez, K. J., McCluskey, C. S., Russell, L. M., McCoy, I. L., Atlas, R. L., Bardeen, C. G., Moore, K. A., Hill, T. C. J., Humphries, R. S., Keywood, M. D., Ristovski, Z., Cravigan, L., Schofield, R., Fairall, C., Mallet, M. D., Kreidenweis, S. M., Rainwater, B., D'Alessandro, J., Wang, Y., Wu, W., Saliba, G., Levin, E. J. T., Ding, S., Lang, F., Truong, S. C. H., Wolff, C., Haggerty, J., Harvey, M. J., Klekociuk, A. R., and McDonald, A.: Observations of Clouds, Aerosols, Precipitation, and Surface Radiation over the Southern Ocean: An Overview of CAPRICORN, MARCUS, MICRE, and SOCRATES, *Bulletin of the American Meteorological Society*, 102, E894–E928, <https://doi.org/10.1175/BAMS-D-20-0132.1>, publisher: American Meteorological Society Section: Bulletin of the American Meteorological Society, 2021.
- 875 Meinander, O., Dagsson-Waldhauserova, P., Amosov, P., Aseyeva, E., Atkins, C., Baklanov, A., Baldo, C., Barr, S. L., Barzycka, B., Benning, L. G., Cvetkovic, B., Enchilik, P., Frolov, D., Gassó, S., Kandler, K., Kasimov, N., Kavan, J., King, J., Koroleva, T., Krupskaya, V., Kulmala, M., Kusiak, M., Lappalainen, H. K., Laska, M., Lasne, J., Lewandowski, M., Luks, B., McQuaid, J. B., Moroni, B., Murray, B., Möhler, O., Nawrot, A., Nickovic, S., O'Neill, N. T., Pejanovic, G., Popovicheva, O., Ranjbar, K., Romanias, M., Samonova, O., Sanchez-Marroquin, A., Schepanski, K., Semerkov, I., Sharapova, A., Shevnina, E., Shi, Z., Sofiev, M., Thevenet, F., Thorsteinsson, T., Timofeev, M., Umo, N. S., Uppstu, A., Urupina, D., Varga, G., Werner, T., Arnalds, O., and Vukovic Vimic, A.: Newly identified climatically and environmentally significant high-latitude dust sources, *Atmospheric Chemistry and Physics*, 22, 11 889–11 930, <https://doi.org/10.5194/acp-22-11889-2022>, publisher: Copernicus GmbH, 2022.
- 880 MODIS Land Science Team: MODIS/Terra Atmospherically Corrected Surface Reflectance 5-Min L2 Swath 250m, 500m, 1km, <https://doi.org/10.5067/MODIS/MOD09.061>, 2020.
- 885 Moore, K. A., Hill, T. C. J., McCluskey, C. S., Twohy, C. H., Rainwater, B., Toohey, D. W., Sanchez, K. J., Kreidenweis, S. M., and DeMott, P. J.: Characterizing Ice Nucleating Particles Over the Southern Ocean Using Simultaneous Aircraft and Ship Observations, *Journal of Geophysical Research: Atmospheres*, 129, e2023JD039 543, <https://doi.org/10.1029/2023JD039543>, [eprint: https://onlinelibrary.wiley.com/doi/pdf/10.1029/2023JD039543](https://onlinelibrary.wiley.com/doi/pdf/10.1029/2023JD039543), 2024.
- 890

- Morrison, H., de Boer, G., Feingold, G., Harrington, J., Shupe, M. D., and Sulia, K.: Resilience of persistent Arctic mixed-phase clouds, *Nature Geoscience*, 5, 11–17, <https://doi.org/10.1038/ngeo1332>, 2012.
- Murray, B. J., Haddrell, A. E., Peppe, S., Davies, J. F., Reid, J. P., O’Sullivan, D., Price, H. C., Kumar, R., Saunders, R. W., Plane, J. M. C., Umo, N. S., and Wilson, T. W.: Glass formation and unusual hygroscopic growth of iodine acid solution droplets with relevance for iodine mediated particle formation in the marine boundary layer, *Atmospheric Chemistry and Physics*, 12, 8575–8587, <https://doi.org/10.5194/acp-12-8575-2012>, publisher: Copernicus GmbH, 2012a.
- Murray, B. J., O’Sullivan, D., Atkinson, J. D., and Webb, M. E.: Ice nucleation by particles immersed in supercooled cloud droplets, *Chemical Society Reviews*, 41, 6519–6554, <https://doi.org/10.1039/C2CS35200A>, publisher: The Royal Society of Chemistry, 2012b.
- Murray, B. J., Carslaw, K. S., and Field, P. R.: Opinion: Cloud-phase climate feedback and the importance of ice-nucleating particles, *Atmospheric Chemistry and Physics*, 21, 665–679, <https://doi.org/10.5194/acp-21-665-2021>, publisher: Copernicus GmbH, 2021.
- Murray-Watson, R. J. and Gryspeerdt, E.: Air mass history linked to the development of Arctic mixed-phase clouds, *EGUsphere*, pp. 1–27, <https://doi.org/10.5194/egusphere-2024-129>, publisher: Copernicus GmbH, 2024.
- Murray-Watson, R. J., Gryspeerdt, E., and Goren, T.: Investigating the development of clouds within marine cold-air outbreaks, *Atmospheric Chemistry and Physics*, 23, 9365–9383, <https://doi.org/10.5194/acp-23-9365-2023>, publisher: Copernicus GmbH, 2023.
- Niemand, M., Möhler, O., Vogel, B., Vogel, H., Hoose, C., Connolly, P., Klein, H., Bingemer, H., DeMott, P., Skrotzki, J., and Leisner, T.: A Particle-Surface-Area-Based Parameterization of Immersion Freezing on Desert Dust Particles, *Journal of the Atmospheric Sciences*, 69, 3077–3092, <https://doi.org/10.1175/JAS-D-11-0249.1>, publisher: American Meteorological Society Section: Journal of the Atmospheric Sciences, 2012.
- O’Sullivan, D., Adams, M. P., Tarn, M. D., Harrison, A. D., Vergara-Temprado, J., Porter, G. C. E., Holden, M. A., Sanchez-Marroquin, A., Carotenuto, F., Whale, T. F., McQuaid, J. B., Walshaw, R., Hedges, D. H. P., Burke, I. T., Cui, Z., and Murray, B. J.: Contributions of biogenic material to the atmospheric ice-nucleating particle population in North Western Europe, *Scientific Reports*, 8, 13 821, <https://doi.org/10.1038/s41598-018-31981-7>, number: 1 Publisher: Nature Publishing Group, 2018.
- Pereira Freitas, G., Adachi, K., Conen, F., Heslin-Rees, D., Krejci, R., Tobo, Y., Yttri, K. E., and Zieger, P.: Regionally sourced bioaerosols drive high-temperature ice nucleating particles in the Arctic, *Nature Communications*, 14, 5997, <https://doi.org/10.1038/s41467-023-41696-7>, publisher: Nature Publishing Group, 2023.
- Petters, M. D. and Wright, T. P.: Revisiting ice nucleation from precipitation samples, *Geophysical Research Letters*, 42, 8758–8766, <https://doi.org/10.1002/2015GL065733>, _eprint: <https://onlinelibrary.wiley.com/doi/pdf/10.1002/2015GL065733>, 2015.
- Pithan, F., Svensson, G., Caballero, R., Chechin, D., Cronin, T. W., Ekman, A. M. L., Neggers, R., Shupe, M. D., Solomon, A., Tjernström, M., and Wendisch, M.: Role of air-mass transformations in exchange between the Arctic and mid-latitudes, *Nature Geoscience*, 11, 805–812, <https://doi.org/10.1038/s41561-018-0234-1>, number: 11 Publisher: Nature Publishing Group, 2018.
- Porter, G. C. E., Adams, M. P., Brooks, I. M., Ickes, L., Karlsson, L., Leck, C., Salter, M. E., Schmale, J., Siegel, K., Sikora, S. N. F., Tarn, M. D., Vüllers, J., Wernli, H., Zieger, P., Zinke, J., and Murray, B. J.: Highly Active Ice-Nucleating Particles at the Summer North Pole, *Journal of Geophysical Research: Atmospheres*, 127, e2021JD036 059, <https://doi.org/10.1029/2021JD036059>, _eprint: <https://onlinelibrary.wiley.com/doi/pdf/10.1029/2021JD036059>, 2022.
- Prenni, A. J., Harrington, J. Y., Tjernström, M., DeMott, P. J., Avramov, A., Long, C. N., Kreidenweis, S. M., Olsson, P. Q., and Verlinde, J.: Can Ice-Nucleating Aerosols Affect Arctic Seasonal Climate?, *Bulletin of the American Meteorological Society*, 88, 541–550, <https://doi.org/10.1175/BAMS-88-4-541>, publisher: American Meteorological Society Section: Bulletin of the American Meteorological Society, 2007.

- Price, H. C., Baustian, K. J., McQuaid, J. B., Blyth, A., Bower, K. N., Choullarton, T., Cotton, R. J., Cui, Z., Field, P. R., Gallagher,
930 M., Hawker, R., Merrington, A., Miltenberger, A., Neely III, R. R., Parker, S. T., Rosenberg, P. D., Taylor, J. W., Trembath, J.,
Vergara-Temprado, J., Whale, T. F., Wilson, T. W., Young, G., and Murray, B. J.: Atmospheric Ice-Nucleating Particles in the Dusty
Tropical Atlantic, *Journal of Geophysical Research: Atmospheres*, 123, 2175–2193, <https://doi.org/10.1002/2017JD027560>, _eprint:
<https://onlinelibrary.wiley.com/doi/pdf/10.1002/2017JD027560>, 2018.
- Rahn, K. A., Borys, R. D., and Shaw, G. E.: The Asian source of Arctic haze bands, *Nature*, 268, 713–715, <https://doi.org/10.1038/268713a0>,
935 publisher: Nature Publishing Group, 1977.
- Rinaldi, M., Hiranuma, N., Santachiara, G., Mazzola, M., Mansour, K., Paglione, M., Rodriguez, C. A., Traversi, R., Becagli, S., Cappel-
letti, D., and Belosi, F.: Ice-nucleating particle concentration measurements from Ny-Ålesund during the Arctic spring–summer in 2018,
Atmospheric Chemistry and Physics, 21, 14 725–14 748, <https://doi.org/10.5194/acp-21-14725-2021>, publisher: Copernicus GmbH, 2021.
- Rogers, D. C., DeMott, P. J., and Kreidenweis, S. M.: Airborne measurements of tropospheric ice-nucleating aerosol particles in the
940 Arctic spring, *Journal of Geophysical Research: Atmospheres*, 106, 15 053–15 063, <https://doi.org/10.1029/2000JD900790>, _eprint:
<https://onlinelibrary.wiley.com/doi/pdf/10.1029/2000JD900790>, 2001.
- Rosenberg, P. D., Dean, A. R., Williams, P. I., Dorsey, J. R., Minikin, A., Pickering, M. A., and Petzold, A.: Particle sizing calibration with
refractive index correction for light scattering optical particle counters and impacts upon PCASP and CDP data collected during the Fen-
nec campaign, *Atmospheric Measurement Techniques*, 5, 1147–1163, <https://doi.org/10.5194/amt-5-1147-2012>, publisher: Copernicus
945 GmbH, 2012.
- Rymer, K. G., Rachlewicz, G., Buchwal, A., Temme, A. J. A. M., Reimann, T., and van der Meij, W. M.: Contemporary and past aeolian deposition rates in periglacial conditions (Ebba Valley, central Spitsbergen), *CATENA*, 211, 105 974,
<https://doi.org/10.1016/j.catena.2021.105974>, 2022.
- Sanchez-Marroquin, A., Hedges, D. H. P., Hiscock, M., Parker, S. T., Rosenberg, P. D., Trembath, J., Walshaw, R., Burke, I. T., McQuaid,
950 J. B., and Murray, B. J.: Characterisation of the filter inlet system on the FAAM BAe-146 research aircraft and its use for size-resolved
aerosol composition measurements, *Atmospheric Measurement Techniques*, 12, 5741–5763, <https://doi.org/10.5194/amt-12-5741-2019>,
publisher: Copernicus GmbH, 2019.
- Sanchez-Marroquin, A., Arnalds, O., Baustian-Dorsi, K. J., Browse, J., Dagsson-Waldhauserova, P., Harrison, A. D., Maters, E. C., Pringle,
K. J., Vergara-Temprado, J., Burke, I. T., McQuaid, J. B., Carslaw, K. S., and Murray, B. J.: Iceland is an episodic source of atmospheric ice-
955 nucleating particles relevant for mixed-phase clouds, *Science Advances*, 6, eaba8137, <https://doi.org/10.1126/sciadv.aba8137>, publisher:
American Association for the Advancement of Science, 2020.
- Sanchez-Marroquin, A., West, J. S., Burke, I. T., McQuaid, J. B., and Murray, B. J.: Mineral and biological ice-nucleating particles above
the South East of the British Isles, *Environmental Science: Atmospheres*, 1, 176–191, <https://doi.org/10.1039/D1EA00003A>, publisher:
RSC, 2021.
- 960 Sanchez-Marroquin, A., Barr, S. L., Burke, I. T., McQuaid, J. B., and Murray, B. J.: Aircraft ice-nucleating particle and aerosol
composition measurements in the western North American Arctic, *Atmospheric Chemistry and Physics*, 23, 13 819–13 834,
<https://doi.org/10.5194/acp-23-13819-2023>, publisher: Copernicus GmbH, 2023.
- Schmale, J., Baccarini, A., Thurnherr, I., Henning, S., Efraim, A., Regayre, L., Bolas, C., Hartmann, M., Welti, A., Lehtipalo, K., Aemisegger,
F., Tatzelt, C., Landwehr, S., Modini, R. L., Tummon, F., Johnson, J. S., Harris, N., Schnaiter, M., Toffoli, A., Derkani, M., Bukowiecki,
965 N., Stratmann, F., Dommen, J., Baltensperger, U., Wernli, H., Rosenfeld, D., Gysel-Beer, M., and Carslaw, K. S.: Overview of the Antarctic
Circumnavigation Expedition: Study of Preindustrial-like Aerosols and Their Climate Effects (ACE-SPACE), *Bulletin of the American*

- Meteorological Society, 100, 2260–2283, <https://doi.org/10.1175/BAMS-D-18-0187.1>, publisher: American Meteorological Society Section: Bulletin of the American Meteorological Society, 2019.
- Shaw, G. E.: The Arctic Haze Phenomenon, *Bulletin of the American Meteorological Society*, 76, 2403–2414, [https://doi.org/10.1175/1520-0477\(1995\)076<2403:TAHP>2.0.CO;2](https://doi.org/10.1175/1520-0477(1995)076<2403:TAHP>2.0.CO;2), publisher: American Meteorological Society Section: Bulletin of the American Meteorological Society, 1995.
- Shi, Y., Liu, X., Wu, M., Zhao, X., Ke, Z., and Brown, H.: Relative importance of high-latitude local and long-range-transported dust for Arctic ice-nucleating particles and impacts on Arctic mixed-phase clouds, *Atmospheric Chemistry and Physics*, 22, 2909–2935, <https://doi.org/10.5194/acp-22-2909-2022>, publisher: Copernicus GmbH, 2022.
- 975 Song, C., Dall’Osto, M., Lupi, A., Mazzola, M., Traversi, R., Becagli, S., Gilardoni, S., Vratolis, S., Yttri, K. E., Beddows, D. C. S., Schmale, J., Brean, J., Kramawijaya, A. G., Harrison, R. M., and Shi, Z.: Differentiation of coarse-mode anthropogenic, marine and dust particles in the High Arctic islands of Svalbard, *Atmospheric Chemistry and Physics*, 21, 11 317–11 335, <https://doi.org/10.5194/acp-21-11317-2021>, publisher: Copernicus GmbH, 2021.
- Sorooshian, A., Anderson, B., Bauer, S. E., Braun, R. A., Cairns, B., Crosbie, E., Dadashazar, H., Diskin, G., Ferrare, R., Flagan, R. C., Hair, 980 J., Hostetler, C., Jonsson, H. H., Kleb, M. M., Liu, H., MacDonald, A. B., McComiskey, A., Moore, R., Painemal, D., Russell, L. M., Seinfeld, J. H., Shook, M., Smith, W. L., Thornhill, K., Tselioudis, G., Wang, H., Zeng, X., Zhang, B., Ziemba, L., and Zuidema, P.: Aerosol–Cloud–Meteorology Interaction Airborne Field Investigations: Using Lessons Learned from the U.S. West Coast in the Design of ACTIVATE off the U.S. East Coast, *Bulletin of the American Meteorological Society*, 100, 1511–1528, <https://doi.org/10.1175/BAMS-D-18-0100.1>, publisher: American Meteorological Society Section: Bulletin of the American Meteorological Society, 2019.
- 985 Stein, A. F., Draxler, R. R., Rolph, G. D., Stunder, B. J. B., Cohen, M. D., and Ngan, F.: NOAA’s HYSPLIT Atmospheric Transport and Dispersion Modeling System, *Bulletin of the American Meteorological Society*, 96, 2059–2077, <https://doi.org/10.1175/BAMS-D-14-00110.1>, publisher: American Meteorological Society Section: Bulletin of the American Meteorological Society, 2015.
- Steinke, I., Funk, R., Busse, J., Iturri, A., Kirchen, S., Leue, M., Möhler, O., Schwartz, T., Schnaiter, M., Sierau, B., Toprak, E., Ullrich, R., Ulrich, A., Hoose, C., and Leisner, T.: Ice nucleation activity of agricultural soil dust aerosols from Mongolia, Argentina, 990 and Germany, *Journal of Geophysical Research: Atmospheres*, 121, 13,559–13,576, <https://doi.org/10.1002/2016JD025160>, _eprint: <https://onlinelibrary.wiley.com/doi/pdf/10.1002/2016JD025160>, 2016.
- Stohl, A.: Characteristics of atmospheric transport into the Arctic troposphere, *Journal of Geophysical Research: Atmospheres*, 111, <https://doi.org/10.1029/2005JD006888>, _eprint: <https://onlinelibrary.wiley.com/doi/pdf/10.1029/2005JD006888>, 2006.
- Storelvmo, T., Tan, I., and Korolev, A. V.: Cloud Phase Changes Induced by CO₂ Warming—a Powerful yet Poorly Constrained Cloud- 995 Climate Feedback, *Current Climate Change Reports*, 1, 288–296, <https://doi.org/10.1007/s40641-015-0026-2>, 2015.
- Sze, K. C. H., Wex, H., Hartmann, M., Skov, H., Massling, A., Villanueva, D., and Stratmann, F.: Ice-nucleating particles in northern Greenland: annual cycles, biological contribution and parameterizations, *Atmospheric Chemistry and Physics*, 23, 4741–4761, <https://doi.org/10.5194/acp-23-4741-2023>, publisher: Copernicus GmbH, 2023.
- Talbot, R. W., Andreae, M. O., Berresheim, H., Artaxo, P., Garstang, M., Harriss, R. C., Beecher, K. M., and Li, S. M.: Aerosol chemistry during the wet season in central Amazonia: The influence of long-range transport, *Journal of Geophysical Research: Atmospheres*, 95, 16 955–16 969, <https://doi.org/10.1029/JD095iD10p16955>, _eprint: <https://onlinelibrary.wiley.com/doi/pdf/10.1029/JD095iD10p16955>, 1990.
- 1000 Tang, I. N., Tridico, A. C., and Fung, K. H.: Thermodynamic and optical properties of sea salt aerosols, *Journal of Geophysical Research: Atmospheres*, 102, 23 269–23 275, <https://doi.org/10.1029/97JD01806>, _eprint: <https://onlinelibrary.wiley.com/doi/pdf/10.1029/97JD01806>, 1997.

- 1005 Tatzelt, C., Henning, S., Welti, A., Baccarini, A., Hartmann, M., Gysel-Beer, M., van Pinxteren, M., Modini, R. L., Schmale, J., and Stratmann, F.: Circum-Antarctic abundance and properties of CCN and INPs, *Atmospheric Chemistry and Physics*, 22, 9721–9745, <https://doi.org/10.5194/acp-22-9721-2022>, publisher: Copernicus GmbH, 2022.
- Tobo, Y., Adachi, K., DeMott, P. J., Hill, T. C. J., Hamilton, D. S., Mahowald, N. M., Nagatsuka, N., Ohata, S., Uetake, J., Kondo, Y., and Koike, M.: Glacially sourced dust as a potentially significant source of ice nucleating particles, *Nature Geoscience*, 12, 253–258, <https://doi.org/10.1038/s41561-019-0314-x>, number: 4 Publisher: Nature Publishing Group, 2019.
- 1010 Tornow, F., Ackerman, A. S., and Fridlind, A. M.: Preconditioning of overcast-to-broken cloud transitions by riming in marine cold air outbreaks, *Atmospheric Chemistry and Physics*, 21, 12 049–12 067, <https://doi.org/10.5194/acp-21-12049-2021>, publisher: Copernicus GmbH, 2021.
- U.S. National Ice Center, Fetterer, F., Savoie, M., S., H., and Clemente-Colón, P.: Multisensor Analyzed Sea Ice Extent - Northern Hemisphere (MASIE-NH), Version 1, <https://doi.org/10.7265/N5GT5K3K>, 2010.
- 1015 Vali, G.: Quantitative Evaluation of Experimental Results an the Heterogeneous Freezing Nucleation of Supercooled Liquids, *Journal of the Atmospheric Sciences*, 28, 402–409, [https://doi.org/10.1175/1520-0469\(1971\)028<0402:QEOERA>2.0.CO;2](https://doi.org/10.1175/1520-0469(1971)028<0402:QEOERA>2.0.CO;2), publisher: American Meteorological Society Section: *Journal of the Atmospheric Sciences*, 1971.
- Vali, G.: Revisiting the differential freezing nucleus spectra derived from drop-freezing experiments: methods of calculation, applications, and confidence limits, *Atmospheric Measurement Techniques*, 12, 1219–1231, <https://doi.org/10.5194/amt-12-1219-2019>, publisher: Copernicus GmbH, 2019.
- 1020 Vergara-Temprado, J., Murray, B. J., Wilson, T. W., O’Sullivan, D., Browse, J., Pringle, K. J., Ardon-Dryer, K., Bertram, A. K., Burrows, S. M., Ceburnis, D., DeMott, P. J., Mason, R. H., O’Dowd, C. D., Rinaldi, M., and Carslaw, K. S.: Contribution of feldspar and marine organic aerosols to global ice nucleating particle concentrations, *Atmospheric Chemistry and Physics*, 17, 3637–3658, <https://doi.org/10.5194/acp-17-3637-2017>, publisher: Copernicus GmbH, 2017.
- Vergara-Temprado, J., Miltenberger, A. K., Furtado, K., Grosvenor, D. P., Shipway, B. J., Hill, A. A., Wilkinson, J. M., Field, P. R., Murray, B. J., and Carslaw, K. S.: Strong control of Southern Ocean cloud reflectivity by ice-nucleating particles, *Proceedings of the National Academy of Sciences*, 115, 2687–2692, <https://doi.org/10.1073/pnas.1721627115>, publisher: National Academy of Sciences Section: *Physical Sciences*, 2018.
- 1030 Wegener, A.: *Thermodynamik der atmosphäre.*, J. A. Barth, Leipzig, 1911.
- Wendisch, M., Crewell, S., Ehrlich, A., Herber, A., Kirbus, B., Lüpkes, C., Mech, M., Abel, S. J., Akansu, E. F., Ament, F., Aubry, C., Becker, S., Borrmann, S., Bozem, H., Brückner, M., Clemen, H.-C., Dahlke, S., Dekoutsidis, G., Delanoë, J., De La Torre Castro, E., Dorff, H., Dupuy, R., Eppers, O., Ewald, F., George, G., Gorodetskaya, I. V., Grawe, S., Groß, S., Hartmann, J., Henning, S., Hirsch, L., Jäkel, E., Joppe, P., Jourdan, O., Jurányi, Z., Karalis, M., Kellermann, M., Klingebiel, M., Lonardi, M., Lucke, J., Luebke, A., Maahn, M., Maherndl, N., Maturilli, M., Mayer, B., Mayer, J., Mertes, S., Michaelis, J., Michalkov, M., Mioche, G., Moser, M., Müller, H., Neggers, R., Ori, D., Paul, D., Paulus, F., Pilz, C., Pithan, F., Pöhlker, M., Pörtge, V., Ringel, M., Risse, N., Roberts, G. C., Rosenburg, S., Röttenbacher, J., Rückert, J., Schäfer, M., Schäfer, J., Schemann, V., Schirmacher, I., Schmidt, J., Schmidt, S., Schneider, J., Schnitt, S., Schwarz, A., Siebert, H., Sodemann, H., Sperzel, T., Spreen, G., Stevens, B., Stratmann, F., Svensson, G., Tatzelt, C., Tuch, T., Vihma, T., Voigt, C., Volkmer, L., Walbröl, A., Weber, A., Wehner, B., Wetzel, B., Wirth, M., and Zinner, T.: Overview: Quasi-Lagrangian observations of Arctic air mass transformations – Introduction and initial results of the HALO–(AC)³ aircraft campaign, <https://doi.org/10.5194/egusphere-2024-783>, 2024.
- 1040

- Wex, H., Huang, L., Zhang, W., Hung, H., Traversi, R., Becagli, S., Sheesley, R. J., Moffett, C. E., Barrett, T. E., Bossi, R., Skov, H., Hünerbein, A., Lubitz, J., Löffler, M., Linke, O., Hartmann, M., Herenz, P., and Stratmann, F.: Annual variability of ice-nucleating particle concentrations at different Arctic locations, *Atmospheric Chemistry and Physics*, 19, 5293–5311, <https://doi.org/10.5194/acp-19-5293-2019>, publisher: Copernicus GmbH, 2019.
- 1045
- Whale, T. F., Murray, B. J., O’Sullivan, D., Wilson, T. W., Umo, N. S., Baustian, K. J., Atkinson, J. D., Workneh, D. A., and Morris, G. J.: A technique for quantifying heterogeneous ice nucleation in microlitre supercooled water droplets, *Atmospheric Measurement Techniques*, 8, 2437–2447, <https://doi.org/10.5194/amt-8-2437-2015>, publisher: Copernicus GmbH, 2015.
- Williams, A. S., Dedrick, J. L., Russell, L. M., Tornow, F., Silber, I., Fridlind, A. M., Swanson, B., DeMott, P. J., Zieger, P., and Krejci, R.: Aerosol Size Distribution Properties Associated with Cold-Air Outbreaks in the Norwegian Arctic, *EGUsphere*, pp. 1–20, <https://doi.org/10.5194/egusphere-2024-584>, publisher: Copernicus GmbH, 2024.
- 1050
- Wilson, T. W., Ladino, L. A., Alpert, P. A., Breckels, M. N., Brooks, I. M., Browse, J., Burrows, S. M., Carslaw, K. S., Huffman, J. A., Judd, C., Kilhau, W. P., Mason, R. H., McFiggans, G., Miller, L. A., Nájera, J. J., Polishchuk, E., Rae, S., Schiller, C. L., Si, M., Temprado, J. V., Whale, T. F., Wong, J. P. S., Wurl, O., Yakobi-Hancock, J. D., Abbatt, J. P. D., Aller, J. Y., Bertram, A. K., Knopf, D. A., and Murray, B. J.: A marine biogenic source of atmospheric ice-nucleating particles, *Nature*, 525, 234–238, <https://doi.org/10.1038/nature14986>, number: 7568 Publisher: Nature Publishing Group, 2015.
- 1055
- Xi, Y., Xu, C., Downey, A., Stevens, R., Bachelder, J. O., King, J., Hayes, P. L., and Bertram, A. K.: Ice nucleating properties of airborne dust from an actively retreating glacier in Yukon, Canada, *Environmental Science: Atmospheres*, 2, 714–726, <https://doi.org/10.1039/D1EA00101A>, publisher: RSC, 2022.
- 1060
- Yang, X., Pyle, J. A., and Cox, R. A.: Sea salt aerosol production and bromine release: Role of snow on sea ice, *Geophysical Research Letters*, 35, <https://doi.org/10.1029/2008GL034536>, eprint: <https://onlinelibrary.wiley.com/doi/pdf/10.1029/2008GL034536>, 2008.
- Young, G., Jones, H. M., Darbyshire, E., Baustian, K. J., McQuaid, J. B., Bower, K. N., Connolly, P. J., Gallagher, M. W., and Choulaton, T. W.: Size-segregated compositional analysis of aerosol particles collected in the European Arctic during the ACCACIA campaign, *Atmospheric Chemistry and Physics*, 16, 4063–4079, <https://doi.org/10.5194/acp-16-4063-2016>, publisher: Copernicus GmbH, 2016.
- 1065
- Zhao, X., Huang, K., Fu, J. S., and Abdullaev, S. F.: Long-range transport of Asian dust to the Arctic: identification of transport pathways, evolution of aerosol optical properties, and impact assessment on surface albedo changes, *Atmospheric Chemistry and Physics*, 22, 10389–10407, <https://doi.org/10.5194/acp-22-10389-2022>, publisher: Copernicus GmbH, 2022.

c272r6	above cloud	2023-03-16 2022-03-16	12:07:25	12:34:15	2957	71.0	10.5	N/A	Warm-air intrusion conditions.
c273r1	above cloud	2023-03-19 2022-03-19	12:01:25	12:38:51	3403	73.8	11.2	W	
c273r2	below cloud	2023-03-19 2022-03-19	12:54:07	13:13:35	415	73.9	8.7	W	Two short pauses to avoid showers.
c274r1	above cloud	2023-03-21 2022-03-21	13:47:10	14:07:23	2672	71.8	12.6	NW	
c274r3	below cloud	2023-03-21 2022-03-21	15:18:08	15:41:22	165	71.2	19.3	NW	Two short pauses for aircraft turning and one pause to avoid showers.
c275r1	below cloud	2023-03-23 2022-03-23	10:03:37	10:28:22	162	76.5	23.8	N	
c276r2	upstream	2023-03-23 2022-03-23	12:55:29	13:20:29	1711	78.5	22.0	N	
c276r4	below cloud	2023-03-23 2022-03-23	14:32:27	14:55:27	156	74.6	25.2	N	
c277r1	below cloud	2023-03-24 2022-03-24	10:30:52	10:59:06	159	76.7	22.8	N	Two pauses for altitude increases due to poor visibility. Cloud was in the very early stages of formation.
c278r2	upstream	2023-03-24 2022-03-24	13:02:05	13:26:16	1725	78.2	21.3	N	
c278r4	below cloud	2023-03-24 2022-03-24	14:07:00	14:31:56	333	75.1	26.0	N	Two minute pause during aircraft turning due to precipitation.
c279r1	below cloud	2023-03-25 2022-03-25	11:23:21	11:44:12	155	76.9	28.0	N	
c279r2	above cloud	2023-03-25 2022-03-25	11:48:26	12:08:44	1323	75.4	28.0	N	
c280r1	above cloud	2023-03-29 2022-03-29	09:29:00	09:49:17	1573	74.8	21.6	N	
c280r2	below cloud	2023-03-29 2022-03-29	09:59:55	10:15:58	327	74.1	20.6	N	
c280r3	above cloud	2023-03-29 2022-03-29	10:34:01	10:54:06	2013	72.6	19.4	N	Two minute pause during aircraft turning.
c280r4	below cloud	2023-03-29 2022-03-29	11:05:35	11:24:51	334	72.0	19.3	N	One minute pause to avoid showers.

Table 2. Factors of change in the INP concentration at $-15\text{ }^{\circ}\text{C}$ (F_{INP}), ~~total aerosol surface area and~~ INP concentration normalised by surface area at $-15\text{ }^{\circ}\text{C}$ (F_{S}) and total aerosol surface area (F_{aer}) between three pairs of below-cloud filter measurements.

Flight	Upstream <u>Upwind</u> filter	Downstream <u>Downwind</u> filter	$\Delta\varphi$	F_{INP}	F_{S}	F_{aer}
c275/6	c275r1, Sc	c276r4t, Sc	1.92	0.40	0.53 <u>0.52</u>	0.77 <u>0.75</u>
c280	c280r2, Sc	c280r4t, precipitating Cu	2.17	0.35	0.19	1.89 <u>1.85</u>
c281/2	c282r2, Sc	c282r3t, precipitating Sc/Cu	3.58	0.68	0.40 <u>0.39</u>	1.72 <u>1.69</u>

Table B1. Values of parameters that describe INP concentration (N_{INP}) and INP concentration normalised by surface area ($N_{\text{INP}}/S_{\text{aer}}$) using Eqs. B1 and B2 respectively. There is no parametrisation of $N_{\text{INP}}/S_{\text{aer}}$ for flights c271 and c272 due to a lack of aerosol-size data. Similar parametrisations for INP concentration normalised by N_{aer} and V_{aer} , not presented in this paper, can be found with other metadata at <https://doi.org/10.5281/zenodo.11221599>.

Sample ID	N_{INP}				$N_{\text{INP}}/S_{\text{aer}}$			
	$\nu_{\text{INP}}/10^{-2}\text{L}^{-1}$	$T_{\text{max}}/^{\circ}\text{C}$	a	b	$\nu_{\text{S}}/10^6\text{m}^2$	$T_{\text{max}}/^{\circ}\text{C}$	a	b
c271r1	2.524	-7.00	0.843	0.619	-	-	-	-
c271r2	1.964	-6.00	0.975	0.531	-	-	-	-
c271r3	1.760	-7.67	1.050	0.525	-	-	-	-
c272r6	0.492	-6.00	0.607	0.849	-	-	-	-
c273r1	1.087	-6.96	1.031	0.500	3.599 <u>5.692</u>	-6.96	1.031	0.500
c273r2	1.156	-13.00	0.616	0.793	0.199 <u>0.197</u>	-13.00	0.505 <u>0.533</u>	0.852 <u>0.836</u>
c274r1	3.368	-6.64	1.050	0.570	2.678 <u>3.993</u>	-6.64	1.050	0.570
c274r3	0.415	-4.00	0.606	0.818	0.194 <u>0.193</u>	-6.00	0.311	0.956 <u>0.960</u>
c275r1	2.484	-7.00	0.972	0.539	0.546 <u>0.596</u>	-7.00	0.964 <u>0.933</u>	0.540 <u>0.548</u>
c276r2	5.088	-7.00	1.029	0.553	3.275 <u>4.346</u>	-7.00	1.042 <u>1.030</u>	0.548 <u>0.552</u>
c276r4	1.557	-10.00	1.032	0.570	0.492 <u>0.462</u>	-10.00	0.952 <u>1.031</u>	0.592 <u>0.570</u>
c277r1	1.690	-8.00	0.978	0.631	0.403 <u>0.587</u>	-8.00	0.980 <u>0.757</u>	0.630 <u>0.652</u>
c278r2	4.343	-7.00	0.885	0.654	0.813 <u>1.011</u>	-7.00	0.890 <u>0.960</u>	0.652
c278r4	1.095	-5.97	1.050	0.619	0.257 <u>0.273</u>	-5.97	1.050	0.619
c279r1	1.108	-7.00	1.050	0.605	0.259 <u>0.269</u>	-7.00	0.956 <u>0.960</u>	0.630 <u>0.629</u>
c279r2	2.364	-7.00	1.003	0.640	0.756 <u>0.832</u>	-7.00	0.960 <u>1.049</u>	0.653 <u>0.626</u>
c280r1	1.556	-7.00	1.050	0.653	1.326 <u>1.665</u>	-7.00	1.050	0.653
c280r2	3.160	-6.00	0.474	0.903	0.458 <u>0.477</u>	-6.00	0.471 <u>0.474</u>	0.905 <u>0.903</u>
c280r3	1.320	-5.87	1.050	0.624	0.871 <u>1.163</u>	-5.87	1.050	0.624
c280r4	1.291	-7.44	1.050	0.563	0.163	-7.84 <u>-7.81</u>	0.814 <u>0.834</u>	0.623 <u>0.617</u>
c282r1	2.188	-7.00	1.050	0.701	0.749 <u>0.991</u>	-7.00	1.050	0.701
c282r2	1.223	-5.87	1.050	0.630	0.216 <u>0.226</u>	-5.87	1.050	0.630
c282r3	3.707	-7.00	0.426	0.880	0.380 <u>0.368</u>	-7.00	0.432 <u>0.472</u>	0.876 <u>0.847</u>